Recent advances in polyoxometalate-based lanthanide–oxo clusters

Shu-Rong Li, Wei-Dong Liu, La-Sheng Long, Lan-Sun Zheng, and Xiang-Jian Kong ✉

Collaborative Innovation Center of Chemistry for Energy Materials, State Key Laboratory of Physical Chemistry of Solid Surfaces and Department of Chemistry, College of Chemistry and Chemical Engineering, Xiamen University, Xiamen 361005, China

ABSTRACT: Polyoxometalate (POM)-based lanthanide-oxo clusters (LnOCs) are a class of polynuclear lanthanide–oxygen complexes formed by polyoxometalate stabilization through oxygen bridges in which POMs can be viewed as multidentate inorganic ligands. POM-based LnOCs have received interest owing to their interesting structures and potential applications. In this paper, we summarize the classification, synthesis strategies, and properties of POM-based LnOCs. POM-based LnOCs are classified into three main categories according to their metal core element type and quantity: pure 4f clusters, 5d–4f clusters, and 3d–4f clusters. Their synthetic strategies are divided into four categories based on the source of the POM involved in the structural assembly: the lacunary POMs ligand-directed method, the in-situ transformation of lacunary POMs ligand-directed method, the in-situ generation of lacunary POMs ligand-directed method, and mixed synthesis strategies. In addition, the single-molecule magnets of POM-based LnOCs and their proton conduction properties are summarized.

KEYWORDS: polyoxometalates, lanthanide, clusters, synthetic strategy, applications
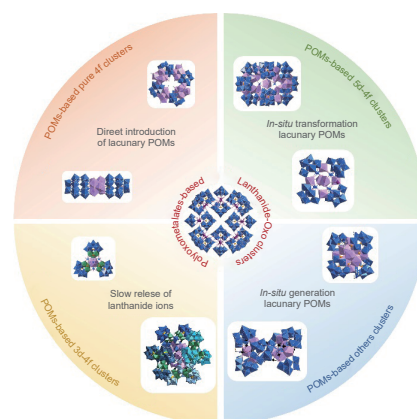
1 Introduction

The special electronic configuration formed by the electron-by-electron filling of 4f orbitals in the inner layers of lanthanides can produce various electronic energy levels, as well as variations in magnetic anisotropy and variable valence states of some metal ions. This special electronic configuration of lanthanides leads to various lanthanide materials with unique properties in optics, magnetism, catalysis, electrochemistry, and so on [1–6]. Lanthanide–oxygen clusters (LnOCs) are polynuclear metal complexes bonded by Ln–O–Ln groups in the structure. They exhibit not only fascinating topologies but also unique properties different from those of individual metal ions and lanthanide nanomaterials due to synergistic and/or coupling interactions within the metal ions [7–12]. Metal clusters offer definite atomic compositions and well-defined geometrical structures, which can be modulated by changing internal atoms and surface ligands [13–17]. Considerable efforts in this field have resulted in the fabrication of a large number of LnOCs based on organic ligands [18–23]. Compared with organic ligand-protected LnOCs, inorganic ligand-protected LnOCs showed higher thermal stability and unique rigid structures

[24–26].

Polyoxometalates (POMs) are a class of metal–oxygen clusters formed by the covalent linkage of high-oxidation-state former transition metals (Mo, W, V, Nb, Ta, etc.) with oxygen atoms. The abundant oxygen atoms on the surface of POMs, especially lacunary POMs with well-defined coordination sites and stronger nucleophilicity, act as coordination sites for lanthanide ions. Thus, lacunary POMs can be used as multidentate inorganic ligands to stabilize LnOCs, forming cluster-to-cluster aggregates [24–33]. POMs are particularly suitable as proton-conducting materials owing to oxygen-rich sites for proton transfer jumps, discrete mobile ionic constituents, and the pseudoliquid phase behavior [27–29]. At the same time, the reversible redox ability of POMs makes them suitable for applications in catalysis, electrochemistry, and energy-related fields [34–40].

Since the POM-based LnOCs $[LnW_{10}O_{35}]^{7-}$ (Ln = La, Ce, Pr, Nd, Sm, Ho, Er, Yb, Y) were first reported in 1971 [41, 42], they have received immense interest owing to their interesting structures and potential applications. To date, large numbers of POM-based LnOCs with various structures and interesting properties have been reported. However, compared with POM-based 3d transition metal clusters and organic ligand-based LnOCs, the development of POM-based LnOCs is still lacking, and the synthesis of high-nuclearity LnOCs has not been demonstrated [18–23, 30–33]. In this review, we summarize the development of the most widely studied LnOCs related to polyoxotungstates, including structural classification,

synthesis strategies, and properties, and briefly discuss their future research directions. This review can assist in the development of the synthesis methods and applications of POM-based LnOCs.

2 Classification of POM-based LnOCs

The reported POM-based LnOCs involve polyoxotungstates, polyoxoniobates, polyoxomolybdates, etc. [43–45]. Here we summarize polyoxotungstate-related LnOCs, which can be classified into three main categories based on the inner metal species of the cluster: pure 4f clusters, d–4f clusters, and p–4f clusters. POM-based d–4f clusters can be further divided into 3d–4f clusters, 4d–4f clusters, and 5d–4f clusters, while only a few 4d–4f clusters and p–4f clusters have been reported. Therefore, we focused on the development of pure 4f clusters, 5d–4f clusters, and 3d–4f clusters in this review.

2.1 POM-based 4f clusters

The simplest POM-based pure 4f cluster is obtained by an Ln^{3+} occupying the vacant site of lacunary POMs. Peacock and Weakley predicted that monolacunary POMs with the Ln cation might form 1:1 and 1:2 clusters (N_{Ln3+}:N_{POMs}) in 1971 [41, 42]. However, it was not until 2000 that Pope et al. obtained the first one-dimensional (1D) chain of the POM group $[Ln(\alpha\text{-}SiW_{11}O_{39})(H_2O)_3]^{5-}$ (Ln = La and Ce) containing 1:1 fragments [46]. Ibrahim et al. reported an isolated 1:1 sandwich-type cluster, $[Ln(H_2O)_nGeW_{11}O_{39}]^{5-}$ (Ln = Dy and Er, n = 4, 3), in 2009 in which the lacunary POMs participate in Ln^{3+} coordination together with H_2O [47]. In the same year, another 1:1 cluster, $[LnH(PW_{11}O_{39})(phen)_2]^{3-}$, was also reported by linking the inorganic ligand $[PW_{11}]$ and 1,10-phenanthroline with Ln^{3+} [48].

The large size of POMs and its coordination-directed effect on lacunary POMs make it easier to obtain the sandwich-type structures of POM-based 4f clusters, commonly 1:2, 2:2, 3:2, 4:2, 5:2, and 6:2 (Table 1). Type 1:2 is usually a mononuclear sandwich-type cluster formed by two monolacunary POMs co-wrapping an Ln^{3+} (Figs. 1(a)–1(c)) [49–51]. In addition, the 1:2 type cluster $[Ln(H_2O)_3(GeW_{10})_2]^{9-}$ (Ln = Ce, Nd, Gd, and Er) was formed by two co-vertex dilacunary POMs $[GeW_{10}]$ sandwiching Ln^{3+} (Fig. 1(d)) [52].

2:2 sandwich-type POM-based 4f clusters comprise two 1:1 POM-based 4f cluster subunits connected by certain linking units. The two subunits can be linked by cross-coordination relying on simple oxygen bridges, such as the cluster $[\{Ce(H_2O)_3(\alpha_2\text{-}P_2W_{17}O_{61})\}_2]^{14-}$ (Fig. 2(a)) published by the Kögerler group in 2019, which can be viewed as monolacunary Dawson POMs $[P_2W_{17}]$ coordinated with Ce^{3+} at the polar position to form the $[Ce(H_2O)_3(\alpha_2\text{-}P_2W_{17}O_{61})]^{7-}$ unit. Two $[Ce(H_2O)_3(\alpha_2\text{-}P_2W_{17}O_{61})]^{7-}$ units were further connected to each other via Ce^{3+} coordination to the terminal O in the adjacent equatorial position $[WO_6]$ [53]. A similar cluster, $[\{Ln(H_2O)_2(\alpha_2\text{-}As_2W_{17}O_{61})\}_2]^{14-}$ (Ln = Dy and Er) (Fig. 2(b)), was published by the Xu group in 2010 [54]. More 2:2 sandwich-type POM-based pure 4f clusters were linked by simple groups (e.g., –OH and halogen ions) or organic ligands (e.g., carboxylic acid ligands or amino acids such as acetate, oxalate, tartrate, and glycine) (Figs. 2(c)–2(i)) [55–61].

The first 3:2 sandwich-type POM-based 4f cluster $[(PW_9O_{34})_2Ce_3O_3(H_2O)_2]^{12-}$ (Fig. 3(a)) was reported in 1986. It comprised two trilacunary POMs $[PW_9]$ wrapped around three head-to-tail-linked Ce^{4+}. Two Ce^{4+} ions were heptacoordinated, and
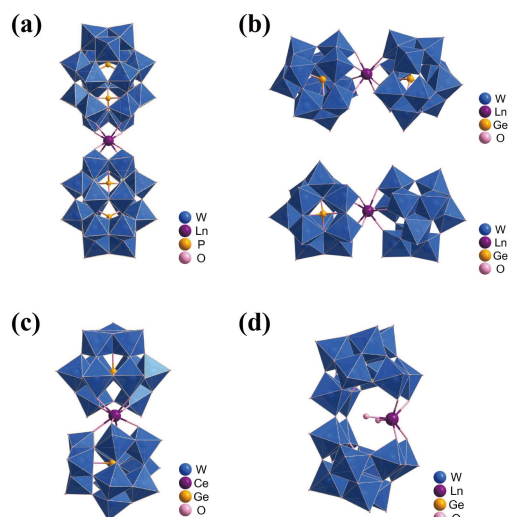

Figure 1 Structures of 1:2 sandwich-type POM-based pure 4f clusters.
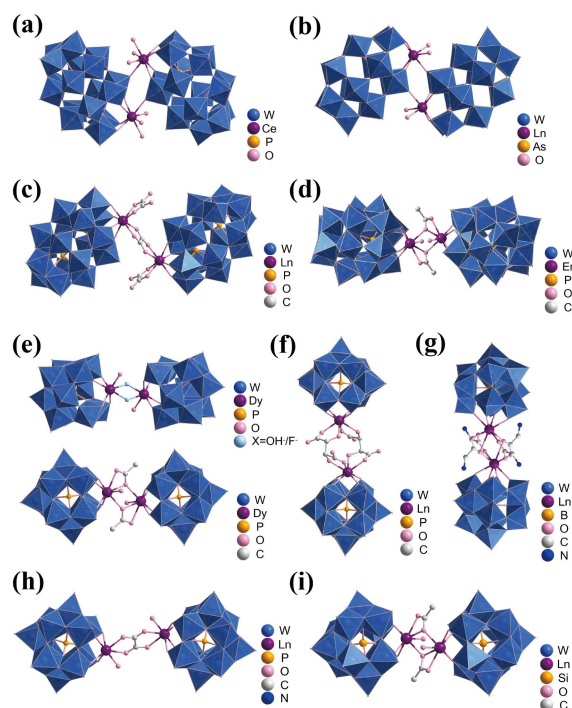

Figure 2 Structures of 2:2 sandwich-type POM-based pure 4f clusters.

the remaining one was hexa-coordinated [62, 63]. Another similar metal cores with the difference that a templating CO_3^{2-} located in the middle of the $[Ln_3O_3]$ triangular ring was reported recently (Figs. 3(b) and 3(c)) [64–67].

4:2 sandwich-type POM-based 3d transition metal–oxygen clusters are one of the most widely studied classes of POM-based metal–oxygen clusters, the most common type being "Finke-type heteropolyacids", which generally consist of two Keggin or Dawson trilacunary POMs with tetranuclear transition metal clusters [68–71]. The related configuration clusters have been studied covering almost all 3d transition metals and multiple trilacunary POMs. Relatively, only a few Ln-containing Finke-type heteropolyacids have been reported. Duval et al. successively obtained five examples using trilacunary POMs $[SiW_9]$ and different O/N-donor organic ligands, which can be regarded as the same planar tetragonal Ce_4 metal core wrapped by two $[SiW_9]$ and

Table 1 Details of the "pure 4f clusters" involved in the manuscript[a]

LnOCs	Logogram	Icon	Synthetic methods
$[Ln(H_2O)_nGeW_{11}O_{39}]^{5-}$ (Ln = Dy, Er, n = 4, 3) [47]	$[LnGeW_{11}]$ (1:1)	—	2
$[LnH(PW_{11}O_{39})(phen)_2]^{3-}$ (Ln = Dy, Er) [48]	$[LnPW_{11}]$ (1:1)	—	1
$[Ln(\alpha-P_2W_{17}O_{61})_2]^{17-}$ (Ln = La, Ce) [49]	$[Ln(P_2W_{17})_2]$ (1:2)	Fig. 1(a)	2
$[Ln(\beta_2-GeW_{11}O_{39})_2]^{13-}$ (Ln = La, Ce, Pr, Nd, Sm, Gd, Dy) [50]	$[Ln(GeW_{11})_2]$ (1:2)	Fig. 1(b)	1
$[Ln(\beta_2-GeW_{11}O_{39})(\alpha-GeW_{11}O_{39})]^{13-}$ (Ln = Ho, Er, Tm) [51]	$[Ln(GeW_{11})_2]$ (1:2)	Fig. 1(b)	1
$[Eu(\alpha-GeW_{11}O_{39})_2]^{13-}$ [49]	$[EuGeW_{11}]$ (1:2)	Fig. 1(c)	3
$[Ln(H_2O)_3(GeW_{10})_2]^{9-}$ (Ln = Ce, Nd, Gd, Er) [52]	$[Ln(GeW_{10})_2]$ (1:2)	Fig. 1(d)	1
$[\{Ce(H_2O)_3(\alpha_2-P_2W_{17}O_{61})\}_2]^{14-}$ [53]	$[(CeP_2W_{17})_2]$ (2:2)	Fig. 2(a)	2
$[\{Ln(H_2O)_2(\alpha_2-As_2W_{17}O_{61})\}_2]^{14-}$ (Ln = Dy, Er) [54]	$[(LnAs_2W_{17})_2]$ (2:2)	Fig. 2(b)	2
$[Ln_2(H_2ox)_2(ox)(\alpha_2-P_2W_{17}O_{61})_2]^{16-}$ (Ln = Ho, Er, Tm, Yb, Y; H_2ox = oxalic acid) [55]	$[(LnP_2W_{17})_2]$ (2:2)	Fig. 2(c)	2
$[\{Er(H_2O)(CH_3COO)(P_2W_{17}O_{61})\}_2]^{16-}$ [56]	$[(ErP_2W_{17})_2]$ (2:2)	Fig. 2(d)	1
$[(PW_{11}O_{39})_2Dy_2X_2(H_2O)_2]^{10-}$ (X = –OH, F⁻, OAc⁻) [57]	$[(DyPW_{11})_2]$ (2:2)	Fig. 2(e)	2
$[Ln(C_4H_2O_6)(\alpha-PW_{11}O_{39})]_2^{16-}$ (Ln = Dy, Ho, Er, Yb, Tm) [58]	$[(LnPW_{11})_2]$ (2:2)	Fig. 2(f)	2
$[Ln_2(Gly)_4(\alpha-BW_{11}O_{39})_2]^{12-}$ (Ln = Ce, Pr, Nd, Sm, Eu, Tm; Gly = glycine) [59]	$[(LnBW_{11})_2]$ (2:2)	Fig. 2(g)	1
$\{[(\alpha-PW_{11}O_{39})Ln(H_2O)]_2(C_2O_4)\}^{10-}$ (Ln = Y, Dy, Ho, Er) [60]	$[(LnPW_{11})_2]$ (2:2)	Fig. 2(h)	1
$[\{Ln(\alpha-SiW_{11}O_{39})(H_2O)\}_2(CH_3COO)_2]^{12-}$ (Ln = Eu, Gd, Tb, Dy, Ho, Er, Tm) [61]	$[(LnSiW_{11})_2]$ (2:2)	Fig. 2(i)	2
$[(PW_9O_{34})_2Ce_3O_3(H_2O)_2]^{12-}$ [62]	$[Ce_3(PW_9)_2]$ (3:2)	Fig. 3(a)	1
$\{[Ln_3O_3(OH_2)_2](PW_9O_{34})_2\}^{15-}$ (Ln = La, Ce) [63]	$[Ln_3(PW_9)_2]$ (3:2)	Fig. 3(a)	1
$[(YOH_2)_3(CO_3)(A-\alpha-PW_9O_{34})_2]^{11-}$ [64]	$[Y_3(PW_9)_2]$ (3:2)	Fig. 3(b)	1
$[(LnOH_2)_3(CO_3)(PW_9O_{34})_2]^{11-}$ (Ln = Y, Tb, Dy, Ho, Er) [64]	$[Ln_3(PW_9)_2]$ (3:2)	Fig. 3(b)	1
$[(SiW_9O_{34})_2(LnH_2O)_3CO_3]^{13-}$ (Ln = Y, Yb) [66]	$[Ln_3(SiW_9)_2]$ (3:2)	Fig. 3(c)	1
$[((GeW_9O_{34})_2(LnH_2O)_3CO_3]^{13-}$ (Ln = Y, Sm, Yb) [65]	$[Ln_3(GeW_9)_2]$ (3:2)	Fig. 3(c)	1
$[(AsW_9O_{34})_2(LnH_2O)_3CO_3]^{11-}$ (Ln = Tb, Dy, Er) [67]	$[Ln_3(AsW_9)_2]$ (3:2)	Fig. 3(b)	1
$[Ce_4(\mu_3-O)_2(SiW_9O_{34})_2(C_5H_8O_2NH_3)_2]^{8-}$ [72]	$[Ce_4(SiW_9)_2]$ (4:2)	Fig. 4(a)	1
$[Ce_4(\mu_3-O)_2(SiW_9O_{34})_2(CH_3COO)_2]^{10-}$ [73]	$[Ce_4(SiW_9)_2]$ (4:2)	Fig. 4(b)	1
$[Ce_4(\mu_3-O)_2(SiW_9O_{34})_2(C_4H_5O_4)_2]^{10-}$ [72]	$[Ce_4(SiW_9)_2]$ (4:2)	—	1
$[Ce_4(\mu_3-O)_2(SiW_9O_{34})_2(C_5H_7O_4)_2]^{10-}$ [72]	$[Ce_4(SiW_9)_2]$ (4:2)	—	1
$[Ce_4(\mu_3-O)_2(SiW_9O_{34})_2(C_6H_{10}O_2NH_3)_2]^{8-}$ [72]	$[Ce_4(SiW_9)_2]$ (4:2)	—	1
$[Ln_2(C_4H_4O_6)(C_4H_2O_6)(AsW_9O_{33})_2]^{18-}$ (Ln = Ho, Er, Tm, Yb. Lu, Y) [75]	$[(Ln_2AsW_9)_2]$ (4:2)	Fig. 4(c)	2
$[Sc_4(H_2O)_{10}(B-\beta-SbW_9O_{33})_2]^{6-}$ [74]	$[Sc_4(SbW_9)_2]$ (4:2)	Fig. 4(d)	1
$[\{Ce(H_2O)\}_2\{Ce(CH_3CN)\}_2(\mu_4-O)(SiW_{10}O_{36})_2]^{6-}$ [76]	$[Ce_4(SiW_{10})_2]$ (4:2)	Fig. 4(e)	1
$[\{Y_4(\mu_3-OH)_4(H_2O)_8(a-P_2W_{15}O_{56})_2]^{16-}$ [77]	$[Y_4(P_2W_{15})_2]$ (4:2)	Fig. 4(f)	1
$[SeO_4Ln_5(H_2O)_7(Se_2W_{14}O_{52})_2]^{13-}$ (Ln = Tb, Dy, Gd, Ho, Er, Tm) [78]	$[Ln_5(Se_2W_{14})_2]$ (5:2)	Fig. 5(a)	3
$[Dy_6(ampH)_4(H_2O)_{23}(ampH_2)(PW_{11}O_{39})_2]$ [79]	$[Dy_6(PW_{11})_2]$ (6:2)	Fig. 5(b)	2
$[\{Yb_6(\mu_6-O)_2(\mu_3-OH)_6(H_2O)_6(a-P_2W_{15}O_{56})_2]^{14-}$ [77]	$[Yb_6(P_2W_{15})_2]$ (6:2)	Fig. 5(c)	1
$[Ce^{IV}_7Ce^{III}_3O_6(OH)_6(CO_3)(H_2O)_{11}(P_2W_{16}O_{59})_3]^{19-}$ [80]	$[Ce_{10}(P_2W_{16})_3]$ (10:3)	Fig. 6(a)	2
$\{[Ln_3(\mu_3-OH)(H_2O)_8AsW_9O_{33}(AsW_{10}O_{35}(mal)]_2\}^{22-}$ (Ln = Sm, Eu, Gd, Tb, Dy, Er; mal = malate) [81]	$[Ln_3(AsW_9)(AsW_{10})]_2$ (3:2)	Fig. 6(b)	2
$\{Ln_{10}(\mu_3-OH)_2(H_2O)_{10}[\alpha(1,8)-GeW_{10}O_{38}]_2[\beta(4,11)-GeW_{10}O_{38}]_2\}^{20-}$ (Ln = La, Ce) [82]	$[Ln_{10}(GeW_{10})_4]$ (10:4)	Fig. 6(c)	2
$[Dy_9(CO_3)_3(ampH)_2(H_2O)_{12}(PW_{10}O_{37})_6]^{35-}$ [79]	$[Dy_3(PW_{10})_2]_3$ (9:6)	Fig. 7(a)	2
$[\{(AsW_9O_{33})Dy(H_2O)_2\}_6]^{36-}$ [83]	$[(DyAsW_9)_6]$ (6:6)	Fig. 7(b)	2
$[\{Ce_6(\mu_3-O)_4(\mu_3-OH)_4(OAc)_2\}(A-\alpha-SiW_9O_{34})_2(\alpha-SiW_{11}O_{39})]^{18-}$ [86]	$[Ce_6(SiW_9)_2(SiW_{11})]$ (6:3)	Fig. 8(a)	2
$[(W_4O_{10})\{(Ce_6(\mu_3-O)_5(\mu_4-O)_3(\mu_2-H_2O))(As^VW_9O_{34})_3\}_2]^{44-}$ (Ce12-2) [84]	$[Ce_{12}(AsW_9)_6]$ (12:6)	Fig. 8(b)	1
$\{[Ce_6(\mu_3-O)_4(\mu_3-OH)_3]_2-(\mu_4-O)_2(CH_3COO)_{13}(SiW_9O_{34})_2\}^{11-}$ (Ce12-1) [85]	$[(Ce_6)_2(SiW_9)_2]$ (12:2)	Fig. 8(c)	1
$[(Ce_6(\mu_4-O)_3(\mu_3-O)_5(\mu_2-H_2O)_3)(HCOO)_3(As^VW_9O_{34})_3]^{22-}$ (Ce6-2) [84]	$[Ce_6(AsW_9)_3]$ (6:3)	Fig. 8(d)	1
$[\{Ce_6(\mu_3-O)_4(\mu_3-OH)_4(HCOO)_{3.5}\}_4(As^{III}W_9O_{33})_4]^{2-}$ (Ce24) [84]	$[(Ce_6AsW_9)_4]$ (24:4)	Fig. 8(e)	1
$[(Ce_6(\mu_3-O)_4(\mu_3-OH)_4)(H_2O)_4(As^{III}W_9O_{33})(HCOO)_9]^{6-}$ (Ce6-1) [84]	$[Ce_6AsW_9]$ (6:1)	Fig. 8(f)	1

[a] In the synthetic methods column: 1 stands for "lacunary POMs ligand-directed method", 2 stands for "*in-situ* transformation lacunary POMs ligand directed method", and 3 stands for "*in-situ* generation lacunary POMs ligand-directed method". In the "Logogram" column, the ratio indicates the N_{Ln3+}:N_{POMs} of the clusters.
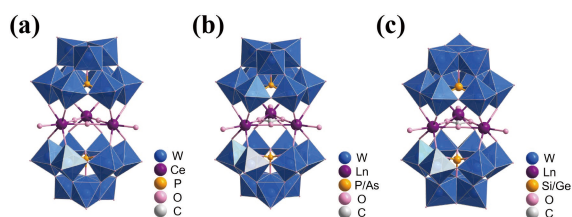
Figure 3 Structures of 3:2 sandwich-type POM-based pure 4f clusters.

two organic ligands, respectively (Figs. 4(a) and 4(b)) [72, 73]. A similar Ln-containing Finke-type heteropolyacid, $[Sc_4(H_2O)_{10}(B-\beta-SbW_9O_{33})_2]^{6-}$ (Fig. 4(d)) [74], was reported in 2017, and a series of clusters $[Ln_2(C_4H_4O_6)(C_4H_2O_6)(AsW_9O_{33})_2]^{18-}$ (Ln = Ho, Er, Tm, Yb, Lu, and Y) (Fig. 4(c)) were published in 2015 [75]. In addition to the planar tetragonal Ln_4 metal core, 4:2 sandwich-type POM-based 4f clusters also have a tetrahedral configuration, such as the cluster $[\{Ce(H_2O)\}_2\{Ce(CH_3CN)\}_2(\mu_4-O)(SiW_{10}O_{36})_2]^{6-}$ (Fig. 4(e)) [76], which comprises a twisted tetrahedral Ce_4 core stabilized by two dilacunary POMs [SiW_{10}]. A similar tetrahedral configuration cluster, $[\{Y_4(\mu_3-OH)_4(H_2O)_8(a-P_2W_{15}O_{56})_2]^{16-}$ (Fig. 4(f)), reported earlier by the Hill group comprised two dilacunary Dawson POMs wrapped around the $[Y_4(OH)_4]$ unit [77].

Sandwich-type POM-based 4f clusters with high nucleation numbers have been rarely reported. A class of 5:2 clusters, $[SeO_4Ln_5(H_2O)_7(Se_2W_{14}O_{52})_2]^{13-}$ (Ln = Tb, Dy, Gd, Ho, Er, and Tm), have been reported by Zhao [78], which comprised two tetralacunary Dawson-type POMs [Se_2W_{14}] wrapped around an Ln_5 cluster. Five Ln^{3+} located on the six vertices of a planar hexagon and the four 100% occupied Ln^{3+} in the middle of the hexagon were connected by one [SeO_4] unit, and the remaining two Ln^{3+} were 50% occupied (Fig. 5(a)). In 2018, Tong and Liu reported a neutral 6:2 cluster $[Dy_6(ampH)_4(H_2O)_{23}(ampH_2)(PW_{11}O_{39})_2]$, which contained the octahedral metal core Dy_6 stabilized by two monolacunary POMs [PW_{11}] and four deprotonated organophosphate ligands (Fig. 5(b)) [79]. The Hill group also
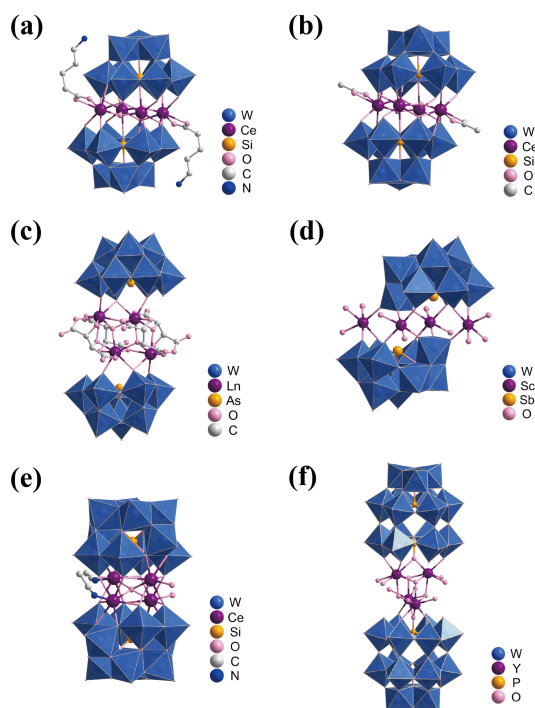
reported similar 6:2 sandwich-type octahedral metal cores, $[\{Yb_6(\mu_6-O)_2(\mu_3-OH)_6(H_2O)_6(a-P_2W_{15}O_{56})_2]^{14-}$, which consisted of two trilacunary POMs [P_2W_{15}] wrapped around the octahedral metal core Yb_6 (Fig. 5(c)) [77].

Higher-nuclearity POM-based pure 4f clusters were obtained by the further assembly of [POM–Ln_m] ($1 \leq m \leq 6$) as sub-building blocks. The trimer $[Ce_7Ce^{III}_3O_6(OH)_6(CO_3)(H_2O)_{11}(P_2W_{16}O_{59})_3]^{19-}$ [80] can be regarded as three trilacunary POMs [P_2W_{16}] linked with two Ce ions to form a [$P_2W_{16}Ce_2$] unit. Three [$P_2W_{16}Ce_2$] units were further assembled by another Ce ion and the [Ce_3CO_3] unit. The metal core [Ce_{10}] has a Keggin-like trilacunary POM structure (Fig. 6(a)), which is the first Keggin-like Ln–O metal framework. They have also reported a series of clusters, $\{[Ln_3(\mu_3-OH)(H_2O)_8(AsW_9O_{33})(AsW_{10}O_{35}(mal))]_2\}^{22-}$ (Ln = Sm, Eu, Gd, Tb, Dy, and Er; mal = malate), which can be regarded as a tetramer of the 3:2 sandwich-type unit $[Ln_3(\mu_3-OH)(H_2O)_8(AsW_9O_{33})(AsW_{10}O_{35})]$ bridged by the organic ligand mal (Fig. 6(b)) [81]. The cluster $\{Ln_{10}(\mu_3-OH)_2(H_2O)_{10}[\alpha(1,8)GeW_{10}O_{38}]_2[\beta(4,11)GeW_{10}O_{38}]_2\}^{20-}$ (Ln = La and Ce) published by the Zheng group in 2019 can be regarded as a centrosymmetric tetramer formed by two 3:2 sandwich-type units and two 2:2 sandwich-type units linked head-to-tail by a shared POM (Fig. 6(c)) [82]. The cluster $Dy_9(CO_3)_3(amphH)_2(H_2O)_{12}(PW_{10}O_{37})_6]^{35-}$ can be regarded as a hexamer formed by the further assembly of three 3:2 sandwich-type units $[Dy_3(CO_3)_3(H_2O)_4(PW_{10}O_{37})_2]$ (Fig. 7(a)). Among them, CO_3^{2-} acts as a template in the formation of the assembly unit [79]. The cluster $[\{(AsW_9O_{33})Dy(H_2O)_2\}_6]^{36-}$ published in 2017 can be regarded as a circular hexamer with S_6 symmetry formed by six mononuclear $[(AsW_9O_{33})Dy(H_2O)_2]$ units linked alternately at the head and tail. Six Dy^{3+} forms a quasi-hexagonal shape, and six trilacunary POMs [AsW_9] are interleaved in the hexagon (Fig. 7(b)) [83].

Nomiya et al. obtained an example of a cluster, $[\{Ce_6(\mu_3-O)_4(\mu_3-OH)_4(OAc)_2\}(A-\alpha-SiW_9O_{34})_2(\alpha-SiW_{11}O_{39})]^{18-}$ (Fig. 8(a)), where the raw material [Si_2W_{18}] was in-situ converted to trilacunary POM [SiW_9] and monolacunary POM [SiW_{11}] POMs. Two [SiW_9], one [SiW_{11}], and two OAc^- together stabilize the metal core $\{Ce_6(\mu_3-O)_4(\mu_3-OH)_4\}$ to form the trimer, and the core metal structure Ce_6 has a similar octahedral configuration with six Ce ions located on the same six vertices of the octahedron. The octahedral configuration Ln_6 is a classical LnOCs metal core structure, which can not only form isolated clusters but also act as assembly units to further form larger clusters. Duval et al. reported a series of clusters
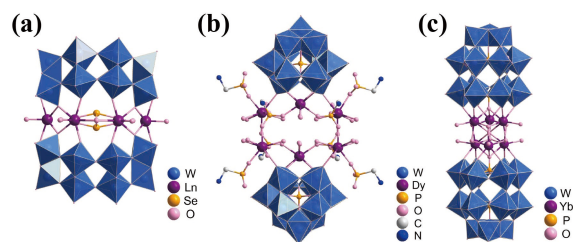

Figure 4 Structures of 4:2 sandwich-type POM-based pure 4f clusters.

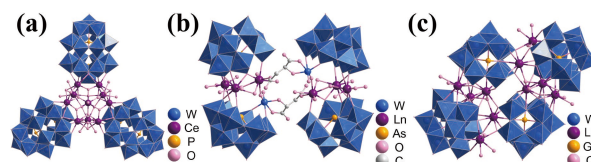**Figure 5** Structures of 5:2 and 6:2 sandwich-type POM-based 4f clusters.

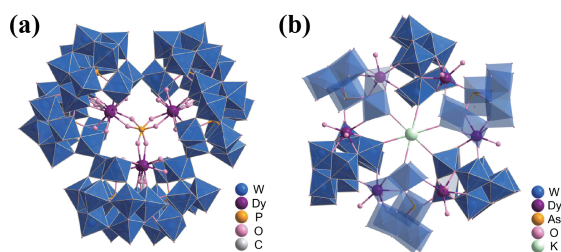**Figure 6** Structures of trimer and tetramer POM-based 4f clusters.

Figure 7 Structures of hexamer POM-based 4f clusters. .

with the octahedral configuration Ln_6 as the assembly unit. The monomer Ce_6-1 is a trilacunary POMs [$As^{III}W_9$] and nine formates involved in stabilizing the octahedral configuration Ce_6-LnOCs (Fig. 8(b)). The cluster Ce_{12}-1 can be regarded as a dimer with a core of Ce_{12} stabilized by two trilacunary POMs [SiW_9] and 13 acetates, where Ce_{12} consists of two octahedral Ce_6 connected by a μ_4-O bridge (Fig. 8(c)). The trimer Ce_6-2 is an octahedral configuration of Ce_6–LnOCs stabilized by three trilacunary POMs [$As^{III}W_{11}$] and three formates (Fig. 8(d)). The hexamer Ce_{12}-2 can be regarded as a further assembly of two clusters Ce_6-2 in which the formate ligand is substituted and the two octahedral Ce_6 are separated by a bicubic alkane [W_8O_{10}] (Fig. 8(f)). Notably, the cluster Ce_{24} can be viewed as a tetramer obtained by the head-to-tail linkage closure of the octahedral configuration Ce_6–LnOCs stabilized by the joint participation of trilacunary POMs [$As^{III}W_9$] (Fig. 8(e)) [84–86].

2.2 POM-based 5d–4f clusters

Compared to POM-based pure 4f clusters, POM-based 5d–4f clusters not only enrich the topology of POM-based LnOCs but also offer the potential to obtain multifunctional POM-based LnOCs. To the best of our knowledge, the reported POM-based 5d–4f clusters involving 5d metals are limited to W. Thus, the POM-
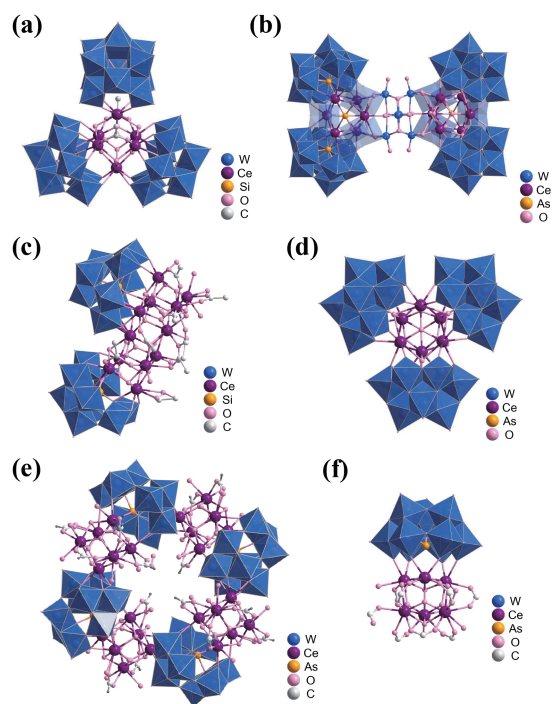

Figure 8 Structures of POM-based 4f clusters with metal cores of octahedral Ce_6 or its further assemblers.

based 5d–4f clusters involved in this review are mainly POM-based W–LnOCs, formed by the introduction of different configurations of tungstates further involved in the assembly based on POM-based 4f clusters (Table 2).

POMs are highly sensitive to pH and prone to reconstruct during the reaction process, while various tungstates are decomposed and further assembled. The reconstructed POMs can be further assembled with tungstates and Ln ions to form POM-based 5d–4f clusters. The precursor [$As_2W_{19}O_{67}(H_2O)$] (Fig. 9) is a classical metastable POM, which can be formed by two trilacunary POMs [B-α-$As^{III}W_9O_{33}$] linked by a [$WO_5(H_2O)$] unit. The presence of [$WO_5(H_2O)$] not only provides the free rotation possibility of [$As_2W_{19}O_{67}(H_2O)$] during the reaction but also facilitates the conversion or decomposition to form lacunary POMs, such as [$As_2W_{19}O_{68}$], [AsW_9], and [AsW_8]. At the same time, the decomposition process releases tungstate fragments that can be further involved in the structural assembly. Thus, [$As_2W_{19}O_{67}(H_2O)$] has been widely reported as a precursor for the construction of POM-based 5d–4f LnOCs [87–91]. Huo et al. obtained two clusters, [($AsW_9O_{33})_6Dy_6W_{10}O_{24}(H_2O)_{23}$]$^{24-}$ and [($AsW_9O_{33})_7W_8Dy_7O_{21}(H_2O)_{17}(\mu_3$-$OH)(OH)$]$^{38-}$, by the reaction of the precursor [$As_2W_{19}O_{67}(H_2O)$] and Dy^{3+} at different pH (2.6 or 6.1). The former can be regarded as a hexameric cluster of six *in-situ* generated trilacunary POMs [B-α-$As^{III}W_9O_{33}$] wrapped around a dumbbell-type metal core [Dy_5W_{10}] (Fig. 9(a)), and the latter is a W-like heptamer comprising a dimer {($AsW_9O_{33})_2W_3Dy_2O_8(H_2O)_7$} unit, a trimer {($AsW_9O_{33})_3W_4Dy_2O_{11}(OH)(H_2O)_3$} unit, and a sandwich-type{($AsW_9O_{33})_2WDy_3O_4(\mu_3$-$OH)(H_2O)_7$} unit linked by μ_2–O bridges with a metal core of [Dy_7W_8] (Fig. 9(b)). The reported [$Ln_4As_5W_{40}O_{144}(H_2O)_{10}(Gly)_2$]$^{21-}$ (Ln = Gd, Tb, Dy, Ho, and Y; Gly = glycine) (Fig. 9(c)) can be regarded as a cluster of four trilacunary POMs [B-α-$As^{III}W_9O_{33}$] and two organic ligands Gly wrapped in a metal core of [Ln_4W_4] in which [B-α-$As^{III}W_9O_{33}$] was also generated by the *in-situ* decomposition of [$As_2W_{19}O_{67}(H_2O)$]. Interestingly, during the synthesis, the cluster [$As_2W_{19}O_{67}(H_2O)$] underwent structural rearrangement to form the [$As_2W_{19}O_{68}$] building block, which occurred with the loss of the terminal water of the linker [$WO_5(H_2O)$] and the change in the angle between two [B-α-$As^{III}W_9O_{33}$] units. This phenomenon also occurs in [{($As_2W_{19}O_{67}(H_2O)$)$Ln(H_2O)_2$}$_2(C_2O_4)$]$^{24-}$ (Ln = Sm, Pr, and Ce) [92], but it only changes the angle of two [B-α-$As^{III}W_9O_{33}$] units. The Boskovic group obtained [$Tb_2(pic)(H_2O)_2(B$-β-$AsW_8O_{30})_2(WO_2(pic))_3$]$^{10-}$ and [$Ln_8(pic)_6(H_2O)_{22}(B$-β-$AsW_8O_{30})_4(WO_2(pic))_6$]$^{12-}$ (Ln = Tb and Eu; pic = 2-picolinate) (Fig. 9(d)) using [$As_2W_{19}O_{67}(H_2O)$] as the precursor, which reconstituted a tetralacunary POM, [(B-β-AsW_8]. The former can be regarded as a cluster of two [(B-β-AsW_8] and four pics cocoordinated with a metal core [Tb_2W_3], whereas the latter can be viewed as a dimer of the former, connected by two crystallographically equivalent [$Ln(pic)(H_2O)_3$] units. Based on the decomposition of [$As_2W_{19}O_{67}(H_2O)$], the Niu group also obtained a cluster, [$Pr_4(H_2O)_6(pzdc)_2As_6W_{58}O_{206}$]$^{38-}$ (pzdc = pyrazine-2,3-dicarboxylic acid) (Fig. 9(e)), which can be seen as a dimer of the {$Pr_2(H_2O)_3(AsW_9O_{33})_3W_2O_4$} unit linked by the pzdc ligand. A similar cluster, [{($AsW_9O_{33})_3Dy_2(H_2O)_4W_4O_9(H_2O)$}$_2(NH_2(CH_2PO_3)_2)$]$^{33-}$ as a dimer of {$Dy_2(H_2O)_4(AsW_9O_{33})_3W_4O_9$} units linked by {$NH_2(CH_2PO_3)_2$} (Fig. 9(f)) was also obtained. Both of the clusters were stabilized by [B-α-$As^{III}W_9O_{33}$] decomposed from [$As_2W_{19}O_{67}(H_2O)$]. [$P_2W_{19}O_{69}(H_2O)$] is a similar metastable dilacunary POM, which is formed by two trilacunary POMs [A-α-

Table 2 Details of the POMs-based "5d–4f clusters" involved in the manuscript

LnOCs	Logogram	Icon	Synthetic methods[a]
$[(AsW_9O_{33})_6Dy_6W_{10}O_{24}(H_2O)_{23}]^{24-}$ [91]	$[Dy_6W_{10}(AsW_9)_6]$	Fig. 9(a)	2
$[(AsW_9O_{33})_7Dy_7W_8O_{21}(H_2O)_{17}(\mu_3\text{-}OH)(OH)]^{38-}$ [91]	$[Dy_7W_8(AsW_9)_7]$	Fig. 9(b)	2
$[Ln_4As_5W_{40}O_{144}(H_2O)_{10}(Gly)_2]^{21-}$ (Ln = Gd, Tb, Dy, Ho, Y) [90]	$[Ln_4W_4(AsW_9)_4]$	Fig. 9(c)	2
$[Tb_2(pic)(H_2O)_2(B\text{-}\beta\text{-}AsW_8O_{30})_2(WO_2(pic))_3]^{10-}$ [89]	$[Tb_2W_3(AsW_8)_2]$	—	2
$[Ln_8(pic)_6(H_2O)_{22}(B\text{-}\beta\text{-}AsW_8O_{30})_4(WO_2(pic))_6]^{12-}$ (Ln = Tb, Eu) [89]	$[Ln_8W_{12}(AsW_8)_4]$	Fig. 9(d)	2
$\{[Pr_2(H_2O)_3(pzdc)As_3W_{29}O_{103}]_2\}^{32-}$ [88]	$[Pr_2W_2(AsW_9)_3]_2$	Fig. 9(e)	2
$[\{(AsW_9O_{33})_3Dy_2(H_2O)_4W_4O_9(H_2O)\}_2(NH_2(CH_2PO_3)_2)]^{33-}$ [87]	$[Dy_2W_4(AsW_9)_3]_2$	Fig. 9(f)	2
$[Dy_8(PW_{10}O_{38})_4(OH)_4(H_2O)_2(W_3O_{14})]^{26-}$ [93]	$[Dy_8W_7(PW_9)_4]$	Fig. 10(a)	2
$[Ln_8(PW_9O_{34})_4(W_7O_{30})]^{30-}$ (Ln = Eu, Y) [94]	$[Ln_8W_7(PW_9)_4]$	Fig. 10(b)	2
$[Gd_6As_6W_{65}O_{229}(OH)_4(H_2O)_{12}(OAc)_2]^{38-}$ [95]	$[Gd_6W_{11}(AsW_9)_6]$	Fig. 11(b)	2
$[Yb_{10}As_{10}W_{88}O_{308}(OH)_8(H_2O)_{28}(OAc)_4]^{40-}$ [95]	$[Yb_{10}W_{16}(AsW_9)_8]$	Fig. 11(c)	2
$[Ln_{27}Ge_{10}W_{106}O_{406}(OH)_4(H_2O)_{24}]^{59-}$ (Ln = La, Ce) [96]	$[Ln@W_6@Ln_{26}@(GeW_{10})_{10}]$	Fig. 12(a)	2
$\{[Ln_3(H_2O)_3(\alpha\text{-}SiW_{11}O_{39})_2]_2\}^{14-}$ (Ln = Sm, Eu, Gd, Tb, Dy) [97]	$[Ln_6W_8(SiW_9)_4]$	Fig. 12(b)	2
$[As^{III}_{12}Ce^{III}_{16}(H_2O)_{36}W_{148}O_{524}]^{76-}$ [98]	$[Ce_{16}W_{20}(W_5O_{18})_4(AsW_9)_{12}]$	Fig. 12(c)	3
$\{[Ce_3W_4O_{10}(H_2O)_9(CH_3COO)_3]_2(Se_2W_7O_{30})(B\text{-}\alpha\text{-}SeW_9O_{33})_4\}^{22-}$ [99]	$[(Ce_3W_4)_2W_7(SeW_9)_4]$	Fig. 13(a)	3
$\{[Se_2Ce_4(H_2O)_8W_4(HPIC)_4O_{10}][B\text{-}\beta\text{-}SeW_8O_{30}]_2[Se_2W_{12}O_{46}]_2\}^{16-}$ [103]	$[Ce_2W_2(Se_2W_{12})(SeW_8)]_2$	Fig. 13(b)	3
$\{[W_2O_5(OH)_2(H_2tart)_2](H_2tart)\{[W_3O_6Ln_2(H_2O)_6][SeW_9O_{33}]_2\}_2\}^{14-}$ (Ln = Eu, Tb, Dy, Ho, Y; H_4tart = D-tartaric acid) [102]	$\{[Ln_2W_3(SeW_9)_2]_2W_2\}$	Fig. 13(c)	3
$\{[W_3Nd_2(H_2O)_3(NO_3)O_6](B\text{-}\alpha\text{-}SeW_9O_{33})_2(\alpha\text{-}Se_2W_{14}O_{52})\}^{17-}$ [100]	$[Nd_2W_3(Se_2W_{14})(SeW_9)]$	Fig. 13(d)	3
$\{[W_2Nd_2(H_2O)_8O_6(OH)_2(\beta\text{-}Se_2W_{14}O_{52})][W_3Nd_2(H_2O)_6O_7(B\text{-}\alpha\text{-}SeW_9O_{33})_2]_2\}^{20-}$ [100]	$[W_5Nd_4(Se_2W_{14})][Nd_2W_3(SeW_9)]_2$	Fig. 13(e)	3
$\{[W_{16}Ln_{10}(H_2O)_{38}O_{50}][B\text{-}\alpha\text{-}SeW_9O_{33}]_8\}^{38-}$ (Ln = La, Ce) [104]	$[Ln_{10}W_{16}(SeW_9)_8]$	Fig. 13(f)	3
$\{[W_{18}Ln_{10}(H_2O)_{34}O_{56}][B\text{-}\alpha\text{-}SeW_9O_{33}]_8\}^{38-}$ (Ln = La, Ce) [104]	$[Ln_{10}W_{18}(SeW_9)_8]$	Fig. 13(g)	3
$[W_{16}Nd_{10}O_{50}(H_2O)_{34}(B\text{-}\alpha\text{-}AsW_9O_{33})_8]^{40-}$ [104]	$[Nd_{10}W_{16}(AsW_9)_8]$	Fig. 13(f)	3
$[W_{16}Pr_8O_{48}(H_2O)_{20}(B\text{-}\alpha\text{-}TeW_9O_{33})_8]^{40-}$ [105]	$[Pr_8W_{16}(TeW_9)_8]$	Fig. 13(h)	3
$[Ln_2(H_2O)_7(W_4O_9)(HPSeW_{15}O_{54})(SeW_9O_{33})_2]^{14-}$ (Ln = Ce, Pr, Nd, Sm, Gd, Tb, Ho, Er) [106]	$[Ln_2W_4(PSeW_{15})(SeW_9)]$	Fig. 13(i)	3
$\{[Ln_4W_4Se_4O_{22}(H_2O)_5](Se_2W_{14}O_{52})_2\}_2^{32-}$ (Ln = Tb, Dy, Ho, Er, Tm, Yb) [101]	$[Ln_4W_4(Se_2W_{14})_2]_2$	Fig. 13(j)	3
$[Yb_4Se_6W_{45}O_{159}(OH)_6(H_2O)_{11}]^{18-}$ [107]	$\{Se_2W_{13}[Yb_2W_2(Se_2W_{14})]_2\}$	Fig. 14(a)	3
$[(\alpha\text{-}SeW_9O_{33})_2\{Ce_2(CH_3COO)(H_2O)_3W_3O_6\}(\alpha\text{-}Se_2W_{14}O_{52})]^{17-}$ [108]	$[Ce_2W_3(Se_2W_{14})(SeW_9)_2]$	Fig. 14(b)	3
$[(\alpha\text{-}SeW_9O_{33})_2\{Ce_2(H_2O)_4W_3O_6\}\{\alpha\text{-}Se_2W_{14}O_{51}(OH)\}]^{15-}$ [108]	$[Ce_2W_3(Se_2W_{14})(SeW_9)_2]$	Fig. 14(c)	3

[a] 1 stands for "lacunary POMs ligand-directed method", 2 stands for "*in-situ* transformation lacunary POMs ligand directed method", and 3 stands for "*in-situ* generation lacunary POMs ligand-directed method".

PW_9O_{34} linked by a $[WO_5(H_2O)]$ unit. $[P_2W_{19}O_{69}(H_2O)]$ was used as a precursor to obtain the cluster $[Dy_8(PW_9O_{34})_4(OH)_4(H_2O)_2(W_7O_{30})]^{26-}$ (Fig. 10), which can be regarded as a metal core $[Dy_8W_7]$ protected by four *in-situ* generated trilacunary POMs $[A\text{-}\alpha\text{-}PW_9]$.

In addition to the above metastable dilacunary POMs, other lacunary POMs are also prone to decomposition during the reaction. The quasi-isomer $[Ln_8(PW_9O_{34})_4(W_7O_{30})]^{30-}$ (Ln = Eu/Y) of $[Dy_8(PW_9O_{34})_4(OH)_4(H_2O)_2(W_7O_{30})]^{26-}$ was obtained using the trilacunary POMs $[A\text{-}\alpha\text{-}PW_9]$ as the precursor, which underwent decomposition during the formation of the cluster [93, 94]. The clusters $[Gd_6As_6W_{65}O_{229}(OH)_4(H_2O)_{12}(OAc)_2]^{38-}$ (Fig. 11(b)) and $[Yb_{10}As_{10}W_{88}O_{308}(OH)_8(H_2O)_{28}(OAc)_4]^{40-}$ (Fig. 11(c)) reported by Kögerler underwent the isomerization of the precursor $[B\text{-}\alpha\text{-}AsW_9]$ to form $[B\text{-}\beta\text{-}AsW_9]$ and co-existed with it during the assembly process. The raw materials and reaction conditions of these clusters were almost identical, indicating that the lanthanide contraction effect and anti-equilibrium cations play an important role in the assembly of POM-based LnOCs [95]. The giant cluster $[Ln_{27}Ge_{10}W_{106}O_{406}(OH)_4(H_2O)_{24}]^{59-}$ ($(Ln@W_6@Ln_{26}@W_{100})$, Ln = La and Ce) (Fig. 12(a)) obtained by the hydrothermal method, which can be seen as a four-shell cluster-in-cluster structure $[Ln_{26}]$ formed by a La^{3+}, a rare $[W_6O_{28}]$ coronal ring, and an elliptic LnOCs wrapped by 10 dilacunary POMs $[GeW_{10}]$ in which the $[GeW_{10}]$ and $[W_6O_{28}]$ units are *in-situ* generated by the decomposition of the raw material trilacunary POM $[GeW_9]$. The cluster is the largest POM-based 5d–4f cluster at present. They also reported another cluster, $\{[Ln_3(H_2O)_3(\alpha\text{-}SiW_{11}O_{39})_2]_2\}^{14-}$ (Ln = Sm, Eu, Gd, Tb, and Dy), in which the metal core is a polyhedral $[Ln_6W_8]$. During the reaction, the precursor $[SiW_9]$ was converted to $[SiW_{11}]$ (Fig. 12(b)) [96, 97].

In addition to the use of some metastable POMs as precursors to obtain POM-based 5d–4f clusters, the one-pot method using simple raw materials is also an effective synthetic strategy [45]. The
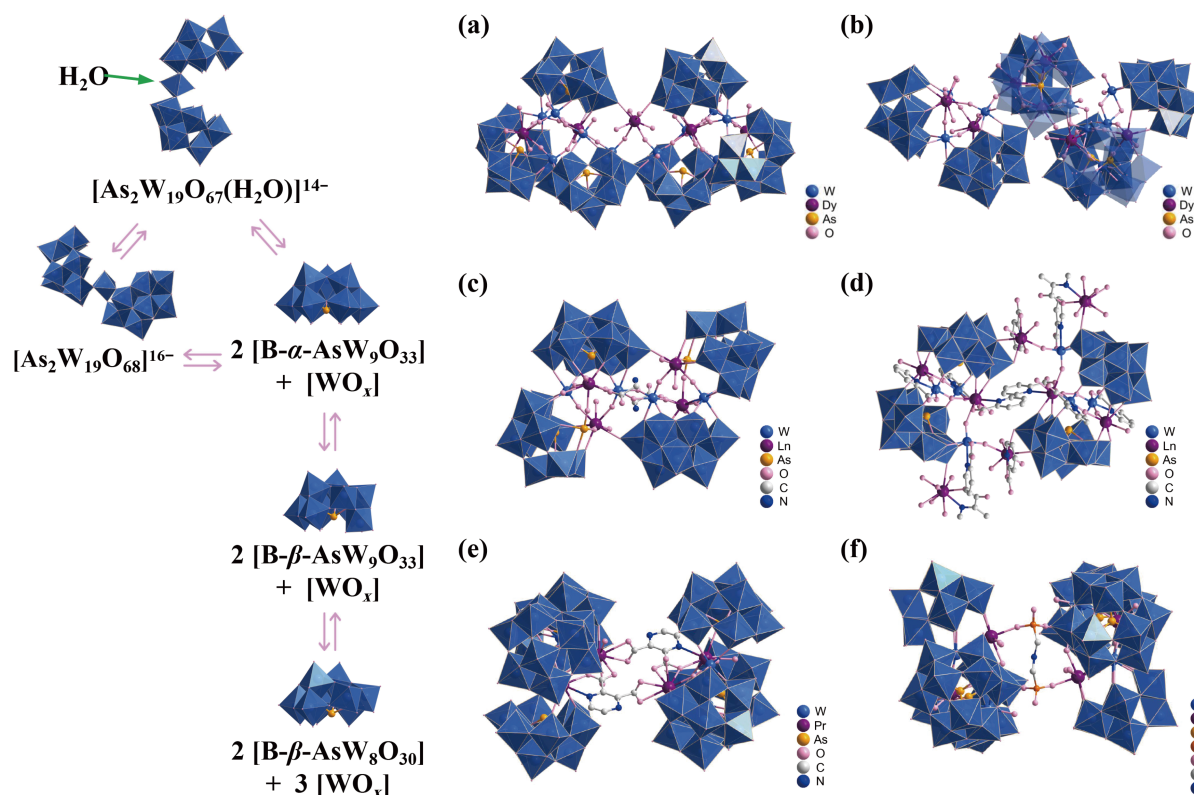
Figure 9 Schematic diagram of the *in-situ* decomposition and recombination of [As$_2$W$_{19}$O$_{67}$(H$_2$O)] and the structures of the partially POM-based 5d–4f clusters obtained by using it as the precursor.

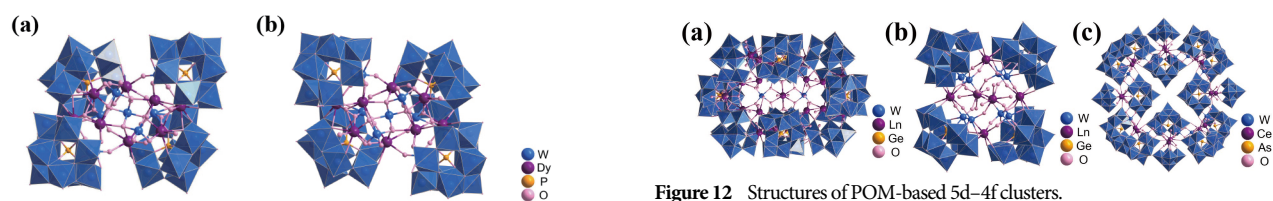**Figure 10** Structures of hexamer POM-based 5d–4f clusters obtained by using [P$_2$W$_{19}$O$_{69}$(H$_2$O)] as a precursor.
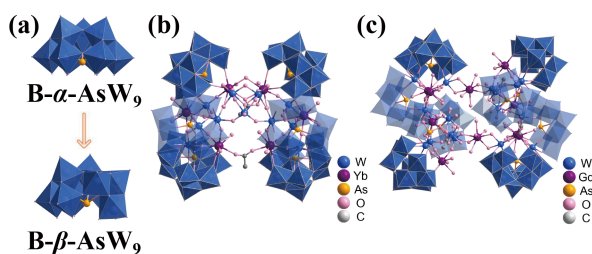
Figure 11 (a) Schematic diagram of the *in-situ* recombination of [B-α-AsW$_9$] with [B-β-AsW$_9$] and ((b) and (c)) the structures of POM-based 5d–4f clusters obtained by using it as a precursor.

Figure 12 Structures of POM-based 5d–4f clusters.

giant ring-like cluster [As$^{III}_{12}$Ce$^{III}_{16}$(H$_2$O)$_{36}$W$_{148}$O$_{524}$]$^{76-}$ (Fig. 12(c)) was formed by the self-assembly method of simple raw materials. 12 trilacunary POMs [AsW$_9$] and 4 [W$_5$O$_{18}$] as mixed inorganic ligands were used, and its metal core [Ce$_{16}$W$_{20}$] ring was formed by four triangular bipyramidal [W$_3$Ce$_2$] and 4 [W$_2$Ce$_2$] [98]. The Zhao group obtained a series of clusters by a one-step synthesis strategy and investigated the effects of pH (3–6) and the types and ratios of raw materials on the structures of the POM-based 5d–4f clusters [99–106]. They obtained the cluster {[Ce$_3$W$_4$O$_{10}$(H$_2$O)$_9$(Ac)$_3$]$_2$

(Se$_2$W$_7$O$_{30}$)(B-α-SeW$_9$O$_{33}$)$_4$}$^{22-}$ (Fig. 13(a)) in an NaAc–HAc solution with a high reactive amount of Na$_2$WO$_4$. WO$_4^{2-}$ not only participates in POM construction but also forms a rare planar [W$_7$] unit, while the [AsO$_3$] unit not only participates in the formation of trilacunary POMs [SeW$_9$] but also acts as an anionic template. They obtained a cluster, {[Se$_2$Ce$_4$(H$_2$O)$_8$W$_4$(HPIC)$_4$O$_{10}$][SeW$_8$O$_{30}$]$_2$ [Se$_2$W$_{12}$O$_{46}$]$_2$}$^{16-}$ (HPIC = 2-picolinic acid) (Fig. 13(b)), using HPIC as an organic auxiliary ligand. In this cluster, there are two inorganic polydentate ligands, the tetralacunary Keggin POM [SeW$_8$] and the hexalacunary Dawson POM [Se$_2$W$_{12}$]. Interestingly, HPIC plays a coordinated chelation role for tungsten ions in this cluster, forming a W–N bond. Using tartaric acid as the organic auxiliary ligand, they obtained {[W$_2$O$_5$(OH)$_2$(H$_2$tart)$_2$](H$_2$tart) {[W$_3$O$_6$Ln$_2$(H$_2$O)$_6$][SeW$_9$O$_{33}$]$_2$}$_2$}$^{14-}$ (Ln = Eu, Tb, Dy, Ho, and Y; H$_4$tart = D-tartaric acid) (Fig. 13(c)). In addition, the clusters {[W$_3$Nd$_2$(H$_2$O)$_3$(NO$_3$)O$_6$](B-α-SeW$_9$O$_{33}$)$_2$(α-Se$_2$W$_{14}$O$_{52}$)}$^{17-}$ and {[W$_2$Nd$_2$(H$_2$O)$_8$O$_6$(OH)$_2$(β-Se$_2$W$_{14}$O$_{52}$)][W$_3$Nd$_2$(H$_2$O)$_6$O$_7$(B-α-SeW$_9$O$_{33}$)$_2$]$_2$}$^{20-}$ (Figs. 13(d) and 13(e)) were prepared by adjusting the ionic strength and pH. Moreover, the effects of different heteroatoms on the cluster structure were studied. When the heteroatoms were Se and As, the clusters {[W$_{16}$Ln$_{10}$(H$_2$O)$_{38}$O$_{50}$][B-α-SeW$_9$O$_{33}$]$_8$}$^{38-}$ (Ln = La, Ce) (Fig. 13(f)) and [W$_{16}$Nd$_{10}$O$_{50}$(H$_2$O)$_{34}$(B-α-AsW$_9$O$_{33}$)$_8$]$^{40-}$ were obtained under different pH conditions, while
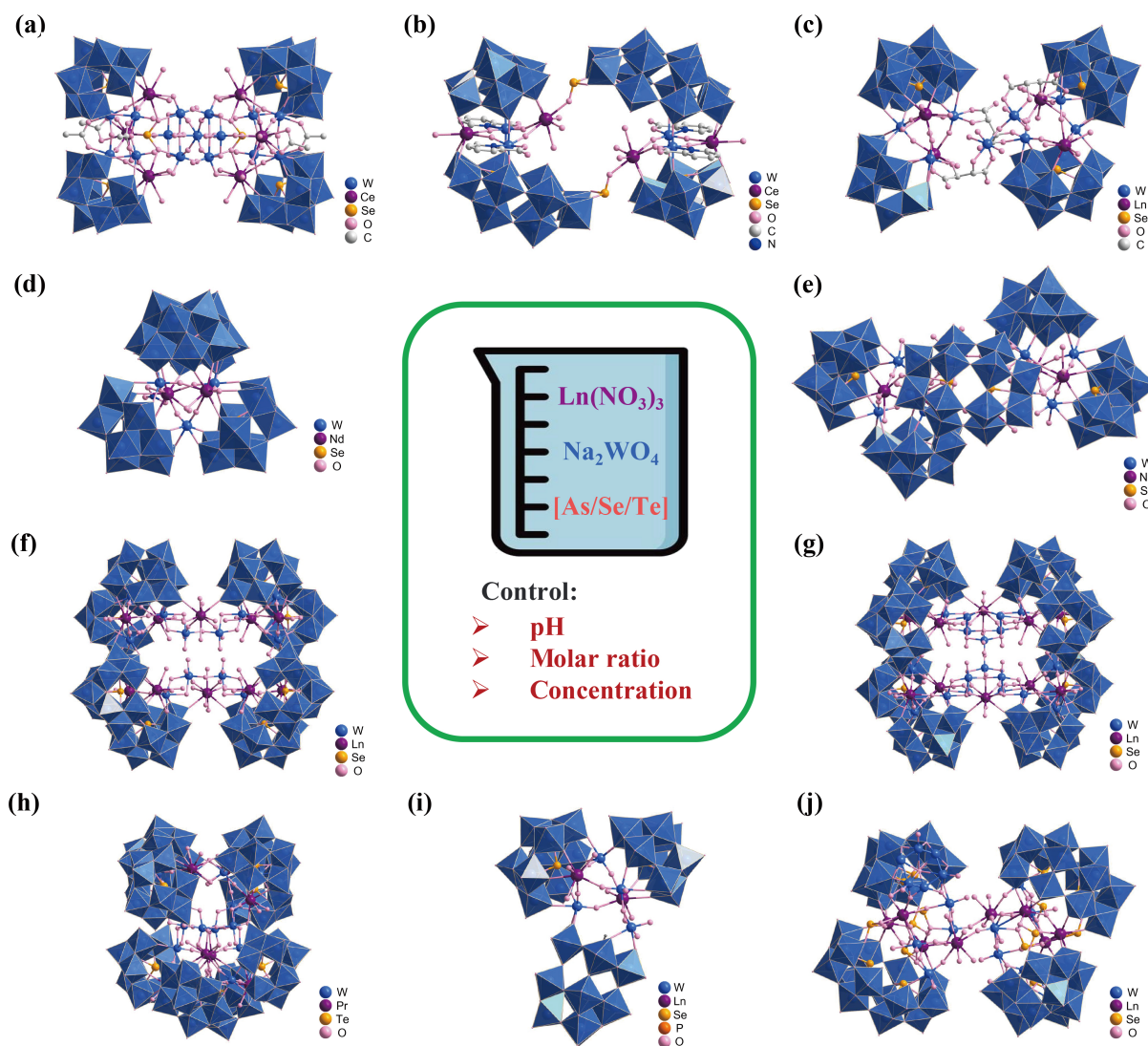
Figure 13 Structures of POM-based 5d–4f clusters obtained by the simple one-pot method.

the cluster $[W_{16}Pr_8O_{48}(H_2O)_{20}(B-\alpha-TeW_9O_{33})_8]^{40-}$ (Fig. 13(h)) was obtained when the heteroatom was Te. Increasing Na_2WO_4 gave the larger cluster $\{[W_{18}Ln_{10}(H_2O)_{34}O_{56}][B-\alpha-SeW_9O_{33}]_8\}^{38-}$ (Ln = La and Ce) (Fig. 13(g)). More interestingly, by adding mixed heteroatomic materials, a series of clusters $[Ln_2(H_2O)_7(W_4O_9)(HPSeW_{15}O_{54})(SeW_9O_{33})_2]^{14-}$ (Ln = Ce, Pr, Nd, Sm, Gd, Tb, Ho, and Er) (Fig. 13(i)) were obtained, including a Dawson-type mixed heteroatomic trilacunary POM, $[PSeW_{15}]$. They obtained the clusters $\{[Ln_4W_4Se_4O_{22}(H_2O)_5](Se_2W_{14}O_{52})_2\}_2^{32-}$ (Ln = Tb, Dy, Ho, Er, Tm, Yb) ((Fig. 13(j)) by increasing the input of Na_2SeO_3 with up to eight $[AsO_3]$ as the linking unit in this cluster. A series of similar clusters, $[Yb_4Se_6W_{45}O_{159}(OH)_6(H_2O)_{11}]^{18-}$ (Fig. 14(a)), $[(\alpha-SeW_9O_{33})_2\{Ce_2(Ac)(H_2O)_3W_3O_6\}(\alpha-Se_2W_{14}O_{52})]^{17-}$ (Fig. 14(b)), and $[(\alpha-SeW_9O_{33})_2\{Ce_2(H_2O)_4W_3O_6\}\{\alpha-Se_2W_{14}O_{51}(OH)\}]^{15-}$ (Fig. 14(c)), were also reported by Su et al. [107, 108]. All of the above clusters are a series of POM-based 5d–4f clusters obtained by the reaction of initial raw tungstate and selenate materials with lanthanide salts, other arsenates (arsenite), tellurates, and the corresponding oxides (As_2O_3, GeO_2) and hydroxides $(Te(OH)_6)$ [109–117]. Currently, either the "in-situ transformation of lacunary POMs ligand-directed method or the simple raw material one-pot method is an effective
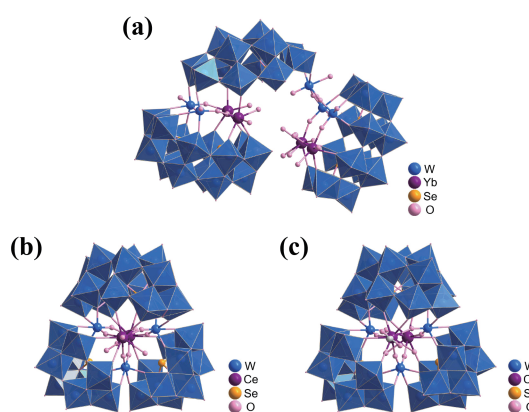

Figure 14 Structures of POM-based pure LnOCs.

method for the synthesis of POM-based 4f–5d clusters. Related research has focused on arsenotungstates and selenotungstates, both of which generally contain triangular biconical $[Ln_2W_3]$ sub-building blocks related to the electronic configurations of these heteroatoms.

2.3 POM-based 3d–4f clusters

Heterometallic 3d–4f clusters have attracted immense interest owing to their interesting optical, electrical, magnetic, and catalytic properties that arise from the interactions of 3d and 4f electrons. Various organic ligand-based 3d–4f clusters with fascinating structures and unique physical and chemical properties have been reported in which organic ligands provide protection and bridge formation [7–12, 118]. Compared with 3d–4f clusters obtained by organic ligand stabilization, inorganic ligand POM-based 3d–4f clusters have higher thermal stability and other unique properties.

So far, POM-based 3d–4f clusters with different structures and excellent properties have also been reported (Table 3). However, due to the coordination competition between 3d metal ions and 4f metal ions with POMs, as well as the strong reaction between 4f ions and oxygen-rich POMs, designing the synthesis of POM-based 3d–4f clusters remains a great challenge [24–26, 33].

In 2008, Fang et al. synthesized the cluster $[\alpha\text{-}P_2W_{16}O_{57}(OH)_2Ce^{IV}Mn^{IV}_6O_9(O_2CCH_3)_8]^{8-}$ (Fig. 15(a)) by reacting the cluster [CeMn₆] as a precursor with the Dawson-type trilacunary POM [P₂W₁₅]. They also reacted [P₂W₁₅] with the cluster $[Ce^{IV}_3Mn^{IV}_2]$ to

Table 3 Details of the "3d–4f clusters" involved in the manuscript

LnOCs	Logogram	Icon	Synthetic methods[a]
$[\alpha\text{-}P_2W_{16}O_{57}(OH)_2Ce^{IV}Mn^{IV}_6O_9(O_2CCH_3)_8]^{8-}$ [119]	[CeMn₆(P₂W₁₆)]	Fig. 15(a)	2
$\{[(\alpha\text{-}P_2W_{15}O_{56})_2Ce_3Mn_2(\mu_3\text{-}O)_4(\mu_2\text{-}OH)_2]_3(\mu_2\text{-}OH)_2(H_2O)_2(PO_4)\}^{47-}$ [120]	[Ce₃Mn₂(P₂W₁₅O₅₆)₂]₃	Fig. 15(b)	1
$\{[CeFe(AsW_{10}O_{38})(H_2O)_2]_3\}^{15-}$ [121]	[CeFe(AsW₁₀)₃]	Fig. 16	3
$[K_9Ln_6Fe_6(H_2O)_{12}(SiW_{10}O_{38})_6]^{26-}$ (Ln = Dy, Tb) [123]	[LnFe(SiW₁₀)₃]	—	2
$[K_9Sm_6Fe_6(H_2O)_{12}(GeW_{10}O_{38})_6]^{26-}$ [124]	[SmFe(GeW₁₀)₃]	—	2
$[K_9Ln_6Cr_6(H_2O)_{12}(GeW_{10}O_{38})_6]^{26-}$ (Ln = Dy, Tb) [122]	[LnCr(GeW₁₀)₃]	—	2
$[\{(GeW_9O_{34})_2Ln_3(H_2O)(OH)_3\}_6\{M_2Ln_3(\mu_3\text{-}OH)_6(OH_2)_6\}_4]^{50-}$ (Ln = Eu, Gd, Dy, Y; M = Zn, Mn, Co) [125–127]	[Ln₃₀W₈(GeW₉)₁₂]	Fig. 17(a)	1
$[\{Ce^{IV}(OAc)\}Cu^{II}_3(H_2O)(B\text{-}\alpha\text{-}GeW_9O_{34})_2]^{11-}$ [128]	[CeCu₃(GeW₉)₂]	Fig. 17(d)	1
$\{[Cu(en)_2(H_2O)][(Cu(en)(OH))_3Ln(SiW_{11}O_{39})(H_2O)]\}_2$ (Ln = Gd, Eu; en = ethylenediamine) [129]	[LnCu₃(SiW₁₁)₂]	Fig. 18(a)	4
$\{[Cu(en)_2(H_2O)][Cu_3Ln(en)_3(OH)_3(H_2O)_2(GeW_{11}O_{39})]\}_2$ (Ln = Eu, Tb, Dy) [130]	[LnCu₃(GeW₁₁)₂]	Fig. 18(b)	4
$\{[Cu(dap)(H_2O)_3][LnCu_3(dap)_3(OH)_3(H_2O)(GeW_{11}O_{39})]\}_2$ (Ln = Sm, Eu, Gd, Tb; dap = 1,2-diaminopropane) [131]	[LnCu₃(GeW₁₁)₂]	Fig. 18(c)	4
$\{[Cu(en)_2(H_2O)][DyCu_3(en)_3(OH)_3(H_2O)_2(GeW_{11}O_{39})]\}_2$ [132]	[DyCu₃(GeW₁₁)₂]	Fig. 18(d)	4
$[LaNi_{12}W_{35}Sb_3P_3O_{139}(OH)_6]^{23-}$ [134]	[LaNi₁₂(PW₉)₃]	Fig. 20(b)	2
$[La_{10}Ni_{48}W_{140}Sb_{16}P_{12}O_{568}(OH)_{24}(H_2O)_{20}]^{86-}$ [134]	[La₁₀Ni₄₈(PW₉)₁₂]	Fig. 20(c)	2
$\{[Fe(C_6H_{16}N_2)Dy(H_2O)_2Fe_2(B\text{-}\alpha\text{-}GeW_9O_{34})(GeW_7O_{29})]_2\}^{20-}$ [135]	[Fe₂Dy(GeW₉)(GeW₇)]₂	Fig. 21(a)	4
$\{[Dy(phen)Fe(B\text{-}\alpha\text{-}GeW_9O_{34})]_2\}^{8-}$ (phen = 1,10-phenanthroline) [135]	[Fe₂Dy₂(GeW₉)₂]	Fig. 21(b)	4
$\{[LnNi_3(OH)_3(B\text{-}\alpha\text{-}SiW_9O_{34})]_4B_{22}O_{42}\}^{34-}$ (Ln = Sm, Gd, Tb) [136]	[LnNi₃(SiW₉)]₄	Fig. 22	1
$[\{LnMn^{III}_4(\mu_3\text{-}O)_2(\mu_2\text{-}OH)_2(H_2O)(CO_3)\}(\beta\text{-}SiW_8O_{31})_2]^{13-}$ (Ln = Ho, Tm, Yb) [138]	[LnMn₄(SiW₈)₂]	Fig. 23(a)	2
$[Ln\{Zn_2PW_{10}O_{38}(H_2O)_2\}_2]^{11-}$ (Ln = Nd, Sm-Lu) [141]	[LnZn₂(PW₁₀)₂]	Fig. 23(b)	2
$\{[Ln(H_2O)_8]_2H_2[Fe_4(H_2O)_4(pic)_4Ge_2W_{20}O_{72}]\}$ (Ln = La, Ce, Nd, Sm, Eu, Gd, Tb, Dy, Er, Tm; Hpic= picolinic acid) [142]	[Ln₂Fe₄(GeW₁₀)₂]	—	4
$\{[Ln(H_2O)_8]_2[Fe_4(H_2O)_8(L\text{-}thr)_2(B\text{-}\beta\text{-}AsW_9O_{33})_2]\}$ (Ln= La, Pr, Nd, Sm, Eu, Gd, Tb, Dy, Er; L-thr = L-threonine) [140]	[Ln₂Fe₄(AsW₉)₂]	—	4
$\{[Gd(H_2O)_8]_4[M(H_2O)_5]_2[M_4(H_2O)_2P_4W_{30}O_{112}]\}$ (M = Mn^{II} and Co^{II}) [146]	[Gd₄Co₆(P₂W₁₅)₂]	—	1
$[FeM_4\{Ln(L)_2\}_2O_2(A\text{-}\alpha\text{-}SiW_9O_{34})_2]$ (M = Mn, Cu; Ln = Gd, Dy, Lu; L = acetylacetonate (acac)) [145]	[FeM₄L₂(SiW₉)₂]	Fig. 23(c)	1
$[FeMn_4\{Lu(L)_2A\}_2O_2(A\text{-}\alpha\text{-}SiW_9O_{34})_2]$ (A = Ag, Na, K) [144]	[FeMn₄Lu₂A₂(SiW₉)₂]	Fig. 23(d)	1
$[Fe_2Ln_2(H_2O)_4(B\text{-}\alpha\text{-}FeW_9O_{34})_2]^{10-}$ (Ln = Dy, Ho, Y) [143]	[Fe₂Ln₂(FeW₉)₂]	Fig. 20(a)	2
$[Ln(H_2O)_8]_2[Fe_4(H_2O)_8(thr)_2][B\text{-}\beta\text{-}SbW_9O_{33}]_2\cdot22H_2O$ (Ln = Pr, Nd, Sm, Eu, Gd, Dy, Lu; thr = threonine) [147]	[Fe₄Ln₂(SbW₉)₂]	Fig. 20(d)	4
$[Ln_3(H_2O)_5M^{II}(H_2O)_3(Sb_4O_4)(SbW_9O_{33})_3(M^{II}W_6O_{24})(WO_2)_3(CH_3COO)]^{17-}$ (Ln = La–Gd, M = Co; Ln = La, Pr, Nd, M = Ni; Ln = Ce, M = Zn) [133, 150]	[Ln₃M₂(SbW₉)₃]	Fig. 19(b)	1
$[Ln_3(H_2O)_3Ni_3(H_2O)_6(SbW_9O_{33})_3(WO_4)(CO_3)]^{16-}$ (Ln = La, Pr, Nd) [133]	[Ln₃Ni₃(SbW₉)₃]	Fig. 19(a)	4
$[Ln_3Ni_9(\mu_3\text{-}OH)_9(SbW_9O_{33})_2(PW_9O_{34})_3(CH_3COO)_3]^{30-}$ (Ln = Dy, Er) [133]	[Ln₃Ni₉(PW₉)₃(SbW₉)₂]	Fig. 19(c)	2
$[M(H_2O)Ln_3(H_2O)_5(W_3O_{11})(SbW_9O_{33})_3]^{20-}$ (M = Co, Ni; Ln= Tb, Dy, Ho, Er, Y) [148]	[Ln₃Ni(SbW₉)₃]	—	2
$[(HPz)_{11}K_4Fe_6Ln(\mu_3\text{-}O)_2(B\text{-}\alpha\text{-}GeW_9O_{34})_2(GeW_6O_{26})]$ (Pz = piperazine, Ln = Tb, Dy, Ho, Er) [151]	[LnFe₆(GeW₉)(GeW₆)]	—	2
$[Eu_{16}Co_7Se_{16}W_{128}O_{448}(CIT)_{10}(HCIT)_2(NO_3)_4(OH)_4(H_2O)_{52}]^{52-}$ (H₄CIT= citric acid) [152]	[Eu₁₆Co₇(Se₂W₁₄)₈]	Fig. 24	4

[a] 1 stands for "lacunary POMs ligand-directed method", 2 stands for "*in-situ* transformation lacunary POMs ligand directed method", and 3 stands for "*in-situ* generation lacunary POMs ligand-directed method", 4 stands for mixing multiple synthesis strategies.
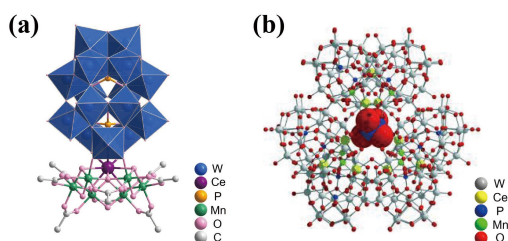
Figure 15 Structures of (a) [α-P$_2$W$_{16}$O$_{57}$(OH)$_2$Ce^{IV}Mn$^{IV}_6$O$_9$(O$_2$CCH$_3$)$_8$]$^{8-}$ and (b) {[(α-P$_2$W$_{15}$O$_{56}$)$_2$Ce$_3$Mn$_2$(μ$_3$-O)$_4$(μ$_2$-OH)$_2$]$_3$(μ$_2$-OH)$_2$(H$_2$O)$_2$(PO$_4$)}$^{47-}$. Reproduced with permission from Ref. [121], © WILEY-VCH Verlag GmbH & Co. KGaA, Weinheim 2008.

obtain the cluster {[(P$_2$W$_{15}$O$_{56}$)$_2$Ce$_3$Mn$_2$O$_4$(OH)$_2$]$_3$(OH)$_2$(H$_2$O)$_2$(PO$_4$)}$^{47-}$ (Fig. 15(b)). These POM-based 3d–4f clusters remain stable compared to the reacting feedstock metal core, and the latter is a trimer formed by the linkage of PO$_4^{3-}$ [119, 120]. In the same year, Wang et al. obtained the cluster {[FeCe(AsW$_{10}$O$_{38}$)(H$_2$O)$_2$]$_3$}$^{15-}$ (Fig. 16) by the *in-situ* synthesis method. The structure of the cluster can be regarded as a trimer of [FeCe(AsW$_{10}$O$_{38}$)(H$_2$O)$_2$] units formed by *in-situ* generated dilacunary POMs [AsW$_{10}$] connected with one Ce^{3+} and one Fe^{3+}. Interestingly, two trimeric polyanions are stacked in a face-to-face rotation of 60°, and they are interconnected by K$^+$ to form petal-like hexameric clusters. The isomorphisms of different types of POMs, cations, and metal ions were also obtained [121–124].

Powell et al. reported a series of clusters, [{(GeW$_9$O$_{34}$)$_2$Ln$_3$(H$_2$O)(OH)$_3$}$_6${M$_2$Ln$_3$(μ$_3$-OH)$_6$(OH$_2$)$_6$}$_4$]$^{56-}$ (Ln = Eu, Gd, Dy, and Y; M = Zn, Mn, and Co) (Fig. 17(a)), which can be regarded as supertetrahedrons. Among them, six classical sandwich-type 3:2 structural units, {(GeW$_9$O$_{34}$)$_2$Ln$_3$(μ$_3$-OH)$_3$(H$_2$O)} (Fig. 17(b)), can be regarded as the six linkers of the tetrahedron, and four triangular biconical {M$_2$Ln$_3$(μ$_3$-OH)$_6$(OH$_2$)$_6$} (Fig. 17(c)) units can be viewed as the four nodes of the tetrahedron [125–127].

Classical metal core fragments [LnM$_3$] were also found in POM-based 3d–4f clusters. The cluster [{Ce^{IV}(OAc)}Cu$^{II}_3$(H$_2$O)(B-α-GeW$_9$O$_{34}$)$_2$]$^{11-}$ (Fig. 17(d)) reported by the Galán-Mascarós group can be viewed as a 4:2 sandwich-type cluster comprising two trilacunary POMs [GeW$_9$] and an OAc$^-$ co-protected wing-like
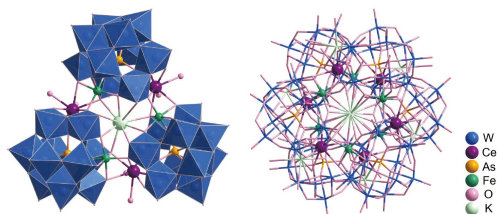
Figure 16 Structures of {[CeFe(AsW$_{10}$O$_{38}$)(H$_2$O)$_2$]$_3$}$^{15-}$ and its dimer.
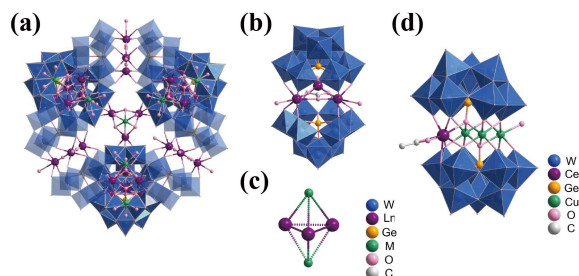
Figure 17 Structures of (a) [{(GeW$_9$O$_{34}$)$_2$Ln$_3$(H$_2$O)(OH)$_3$}$_6${M$_2$Ln$_3$(μ$_3$-OH)$_6$(OH$_2$)$_6$}$_4$]$^{50-}$ and ((b) and (c)) its building blocks. (d) Structure of the cluster [{Ce^{IV}(OAc)}Cu$^{II}_3$(H$_2$O)(B-α-GeW$_9$O$_{34}$)$_2$]$^{11-}$.

[CeCu$_3$] [128]. In comparison, quasi-cubane type [LnM$_3$] units have been reported more frequently, as shown in Fig. 18 [129–132]. The clusters [Ln$_3$Ni$_9$(μ$_3$-OH)$_9$(SbW$_9$O$_{33}$)$_2$(PW$_9$O$_{34}$)$_3$(CH$_3$COO)$_3$]$^{30-}$ (Ln$_3$Ni$_9$, Ln = Dy and Er) can be regarded as pentameric clusters comprising three quasi-cubane [LnNi$_3$] metal cores co-stabilized by two trilacunary POMs [SbW$_9$] and three *in-situ* generated trilacunary POMs [PW$_9$] (Fig. 19(c)). Notably, this is the first 3d–4f cluster containing mixed inorganic POM ligands. In addition, [LaNi$_{12}$W$_{35}$Sb$_3$P$_3$O$_{139}$(OH)$_6$]$^{23-}$ ([LaNi$_{12}$], Fig. 20(b)) and [La$_{10}$Ni$_{48}$W$_{140}$Sb$_{16}$P$_{12}$O$_{568}$(OH)$_{24}$(H$_2$O)$_{20}$]$^{86-}$ ([La$_{10}$Ni$_{48}$], Fig. 20(c)) were reported in 2021 [133, 134]. Among them, the cluster [LaNi$_{12}$] can be regarded as a trimer comprising three *in-situ* generated trilacunary POMs [PW$_9$], one [WO$_4$] unit, and one *in-situ* formed [LaW$_7$O$_{24}$(SbO$_3$)$_3$] unit co-wrapped with the [Ni$_{12}$] unit. The resulting [LaNi$_{12}$] contains three quasi-cubane [Ni$_4$] and one quasi-cubane [LaNi$_3$]. The dodecameric cluster [La$_{10}$Ni$_{48}$] can be structurally regarded as a tetramer of the cluster [LaNi$_{12}$] with four [LaNi$_{12}$] connected to each other by [La$_6$(SbO$_3$)$_4$(H$_2$O)$_{20}$] units. The cluster [La$_{10}$Ni$_{48}$] can be regarded as a supertetrahedron with four
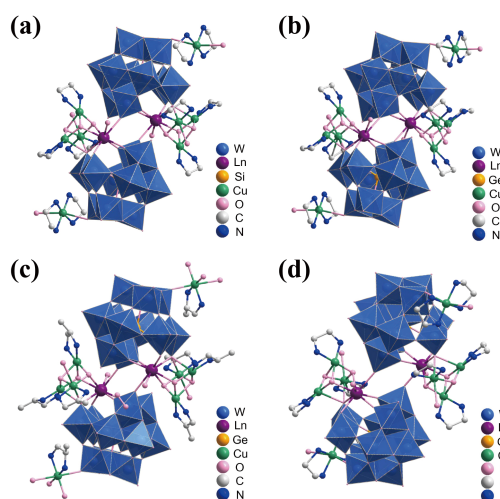
Figure 18 Structures of POM-based 3d–4f clusters containing quasi-cubane LnM$_3$ assembly units.
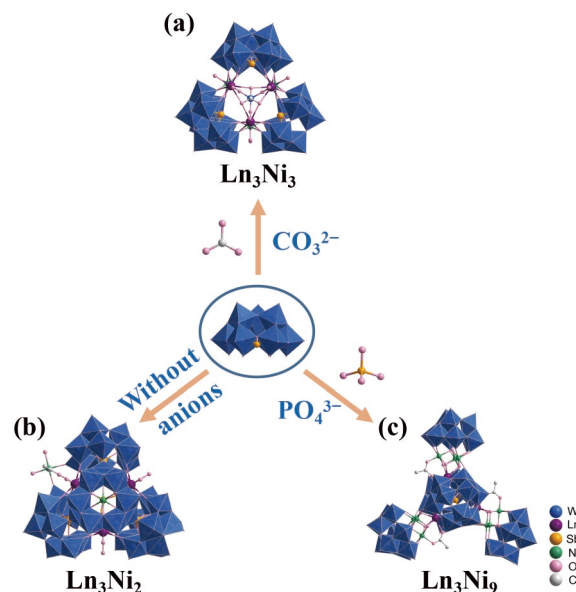
Figure 19 Schematic diagram of anionic template methods.
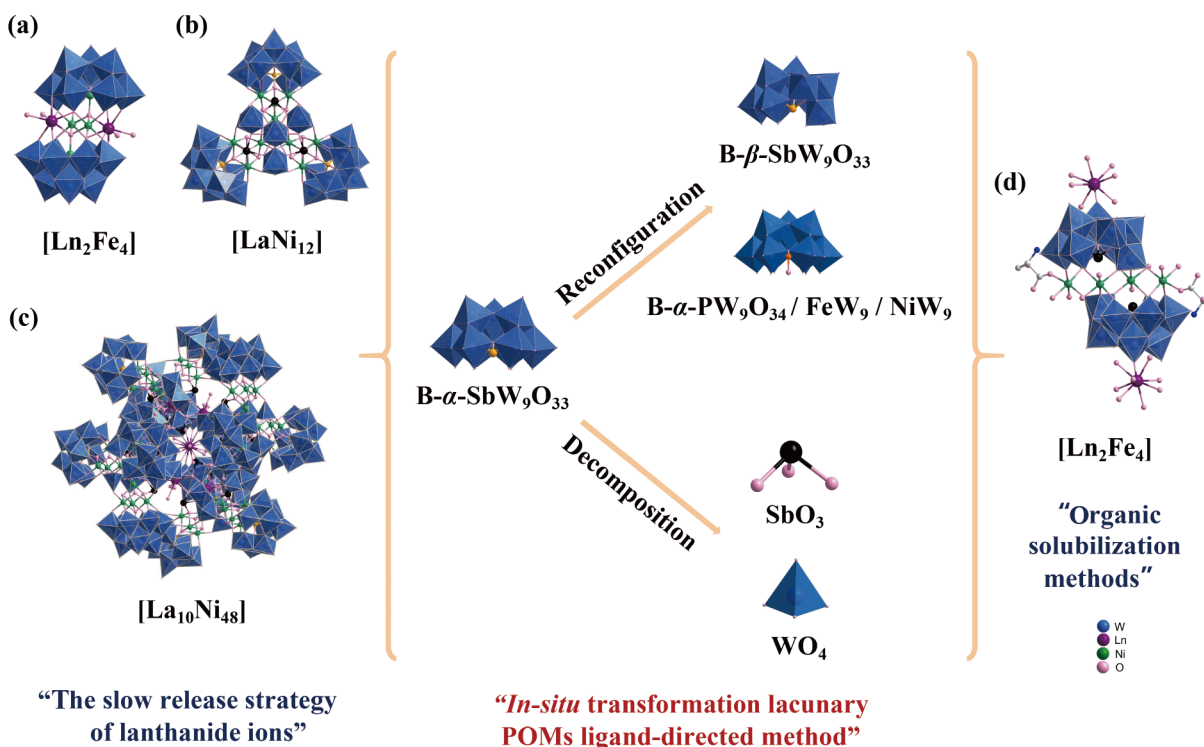
Figure 20 Schematic diagram of mixed synthesis strategies.

[LaNi$_{12}$] located on the four vertices of the tetrahedron, respectively. The cluster [La$_{10}$Ni$_{48}$] is the highest nuclearity POM-based 3d–4f cluster at present. The cluster {[Fe(C$_6$H$_{16}$N$_2$)Dy(H$_2$O)$_2$Fe$_2$(GeW$_9$O$_{34}$)(GeW$_7$O$_{29}$)]$_2$}$^{20-}$ (Fig. 21(a)) reported by the Zheng group in 2020 can be regarded as a dimer of the [Dy(H$_2$O)$_2$Fe$_2$(B-α-GeW$_9$O$_{34}$)(GeW$_7$O$_{29}$)] unit connected by two [Fe(C$_6$H$_{16}$N$_2$)] units, where [Fe$_2$Dy] is a vacancy-containing cubane. They also reported another sandwich-type cluster, {[Dy(phen)Fe(B-α-GeW$_9$O$_{34}$)]$_2$}$^{8-}$ (phen = 1,10-phenanthroline) (Fig. 21(b)), with a [Fe$_4$Dy$_2$] core stabilized by two trilacunary POMs [GeW$_9$] and two phen ligands [135]. In addition, the supertetrahedron {[LnNi$_3$(OH)$_3$(B-α-SiW$_9$O$_{34}$)]$_4$ B$_{22}$O$_{42}$}$^{34-}$ (Ln = Sm, Gd, and Tb) (Fig. 22) can be regarded as a

tetramer comprising four [LnNi$_3$(OH)$_3$(B-α-SiW$_9$O$_{34}$)] units connected by [B$_{22}$O$_{42}$] units, where the [LnNi$_3$(OH)$_3$(B-α-SiW$_9$O$_{34}$)] units are located on the four vertices of the tetrahedron [136].

5:2 sandwich-type clusters [{LnMn$^{III}_4$O$_2$(OH)$_2$(H$_2$O)(CO$_3$)}(SiW$_8$O$_{31}$)$_2$]$^{13-}$ (Ln = Ho, Tm, and Yb) (Fig. 23(a)) with metal cores [LnMn$_4$] were reported by Wang and Zhang et al. [LnMn$_4$] is similar to the classical [CaMn$_4$] configuration in natural photosynthetic systems, except that [Mn$_4$] occupies the cubane configuration site in this cluster, providing a model for the study of artificial photosynthetic systems [137–139]. In addition, other classical sandwich-type POM-based 3d–4f clusters were reported [140–147]. The clusters [Ln{Zn$_2$PW$_{10}$O$_{38}$(H$_2$O)$_2$}$_2$]$^{11-}$ (Ln = Nd, Sm, and Lu) (Fig. 23(b)) can be regarded as sandwich-type clusters involving two [Zn$_2$PW$_{10}$O$_{38}$(H$_2$O)$_2$] units connected by one Ln^{3+},

Figure 21 Structures of POM-based 3d–4f clusters: (a) {[Fe(C$_6$H$_{16}$N$_2$)Dy(H$_2$O)$_2$Fe$_2$(B-α-GeW$_9$O$_{34}$)(GeW$_7$O$_{29}$)]$_2$}$^{20-}$ and (b) {[Dy(phen)Fe(B-α-GeW$_9$O$_{34}$)]$_2$}$^{8-}$.
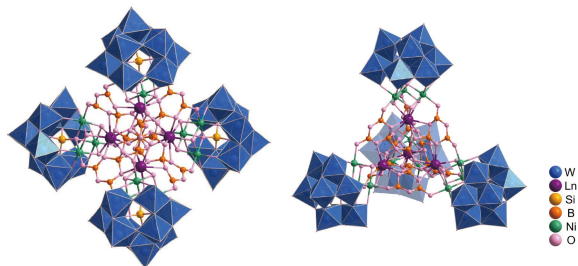
Figure 22 Structures of POM-based 3d–4f clusters {[LnNi$_3$(OH)$_3$(B-α-SiW$_9$O$_{34}$)]$_4$B$_{22}$O$_{42}$}$^{34-}$.

Figure 23 Structures of CaMn$_4$-like clusters and sandwich-type POM-based 3d–4f clusters.

and their metal cores [LnZn$_4$] have a windmill-like appearance. The clusters [FeM$_4${Ln(L)$_2$}$_2$O$_2$(SiW$_9$O$_{34}$)$_2$] (M = Mn and Cu; Ln = Gd, Dy, and Lu; L = acetylacetonate) (Fig. 23(c)) reported by the Mizuno group are relatively rare 7:2 sandwich-type clusters formed by two trilacunary POMs [SiW$_9$]. They also obtained the clusters [FeMn$_4${Lu(L)$_2$A}$_2$O$_2$(SiW$_9$O$_{34}$)$_2$] (A = Ag, Na, and K) (Fig. 23(d)) in a predictable multistep reaction on an automated platform in their subsequent work. The clusters [Fe$_2$Ln$_2$(H$_2$O)$_4$(FeW$_9$O$_{34}$)$_2$]$^{10-}$ (Ln = Dy, Ho, and Y) (Fig. 20(a)) recently reported by the Kong group can be regarded as sandwich-type clusters comprising two *in-situ* generated trilacunary POMs [FeW$_9$] wrapped around wing-like [Fe$_4$Ln$_2$] units, and they are the first POM-based 3d–4f clusters containing a 3d metal heteroatom.

In addition, there are a few POM-based 3d–4f clusters with a supertriangular configuration [133,148–150]. For example, the clusters [Ln$_3$(H$_2$O)$_5$M^{II}(H$_2$O)$_3$(Sb$_4$O$_4$)(SbW$_9$O$_{33}$)$_3$(M^{III}W$_6$O$_{24}$)(WO$_2$)$_3$(CH$_3$COO)]$^{17-}$ (Ln$_3$M$_2$, Ln = La–Gd, M = Co; Ln = La, Pr, and Nd, M = Ni; Ln = Ce, M = Zn) (Fig. 19(b)), [Ln$_3$(H$_2$O)$_3$Ni$_3$(H$_2$O)$_6$(SbW$_9$O$_{33}$)$_3$(WO$_4$)(CO$_3$)]$^{16-}$ (Ln$_3$Ni$_3$, Ln = La, Pr, and Nd) (Fig. 19(a)), [M(H$_2$O)Ln$_3$(H$_2$O)$_5$(W$_3$O$_{11}$)(SbW$_9$O$_{33}$)]$^{20-}$ (M = Co and Ni; Ln = Tb, Dy, Ho, Er, and Y), and [HoCo$_7$Si$_3$W$_{29}$O$_{108}$(OH)$_5$(H$_2$O)$_4$]$^{18-}$ were prepared, respectively. Recently, a series of banana-type clusters, [(HPz)$_{11}$K$_4$Fe$_6$LnO$_2$(GeW$_9$O$_{34}$)$_2$(GeW$_6$O$_{26}$)] (Pz = piperazine; Ln = Tb, Dy, Ho, Er), and the longest POM-based 3d–4f cluster [Eu$_{16}$Co$_7$Se$_{16}$W$_{128}$O$_{448}$(CIT)$_{10}$(HCIT)$_2$(NO$_3$)$_4$(OH)$_4$(H$_2$O)$_{52}$]$^{52-}$ (H$_4$CIT= citric acid) (Fig. 24) were reported by the Zheng group [151, 152].

2.4 Other POM-based clusters

In addition to the above three types of POM-based LnOCs, other types of clusters have also been reported. For example, the 4p–4f cluster {[(H$_4$pic)$_4$Eu$_{10}$Se$_{13}$O$_{28}$(H$_2$O)$_{12}$](α-GeW$_9$O$_{34}$)$_4$}$^{18-}$ (H$_4$pic = isonicotinic acid) shows an interesting multishell layer structure [Se@Eu$_4$@Eu$_6$@{Se$_3$(a-GeW$_9$O$_{34}$)$_4$] [153]. The 5p–4f clusters {H$_{17}$(H$_2$en)$_3$[Sb$^{III}_9$Sb^{V}Ln$_3$O$_{14}$(H$_2$O)$_3$][(SbW$_9$O$_{33}$)$_3$(PW$_9$O$_{34}$)]} (Ln = Ce, Sm, Eu, Gd, Tb, and Dy) and {H$_{13}$(HIm)$_4$K$_2$Na$_4$(H$_2$O)$_9$[Sb$^{III}_9$Sb^{V}Ln$_3$O$_{14}$(H$_2$O)$_3$][(SbW$_9$O$_{33}$)$_3$(PW$_9$O$_{34}$)]} (Ln = Sm, Eu, Gd, Tb, and Dy; Im = imidazole) protected by mixed trilacunary POMs [SbW$_9$] and [PW$_9$] have also been reported [154]. A class of 5p–4f clusters, {[Ln$_4$(H$_2$O)$_6$Sb$_6$O$_4$](SbW$_{10}$O$_{37}$)$_2$(SbW$_8$O$_{31}$)$_2$}$^{22-}$ (Ln = Gd, Tb, Dy, Ho, Er, Tm, Yb, Lu, and Y) [155], and 5p–5d–4f clusters {[Sb$_4$O$_4$Ln$_3$(H$_2$O)$_8$W$_2$O$_4$(H$_2$O)$_2$(B-α-SbW$_9$O$_{33}$)$_4$]$_2$} (Ln = Dy, Ho, and Y) [156], [Dy$_3$(H$_2$O)$_6$Sb^V(H$_2$O)(W$_3$O$_{11}$)(B-α-SbW$_9$O$_{33}$)$_3$] [148], and [Sb$_{15}$W$_3$O$_{29}$(OH)$_3$ Tb$_7$O)$_6$(SbW$_8$O$_{30}$)(SbW$_9$O$_{33}$)$_5$]$^{27-}$ [157] have been reported recently.

3 Strategies for the synthesis of POM-based LnOCs

The synthesis of POM-based LnOCs is challenging mainly because
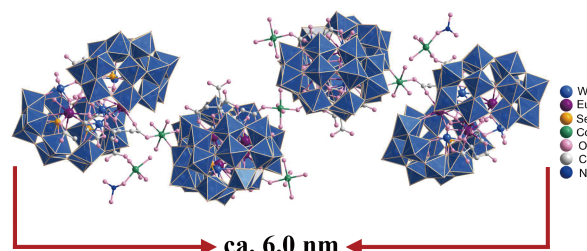
Figure 24 Structure of the cluster [Eu$_{16}$Co$_7$Se$_{16}$W$_{128}$O$_{448}$(CIT)$_{10}$(HCIT)$_2$(NO$_3$)$_4$(OH)$_4$(H$_2$O)$_{52}$]$^{52-}$.

of the complex coordination numbers and variable coordination configurations of Ln ions, as well as the strong reactivity between Ln ions and POMs. The coordination competi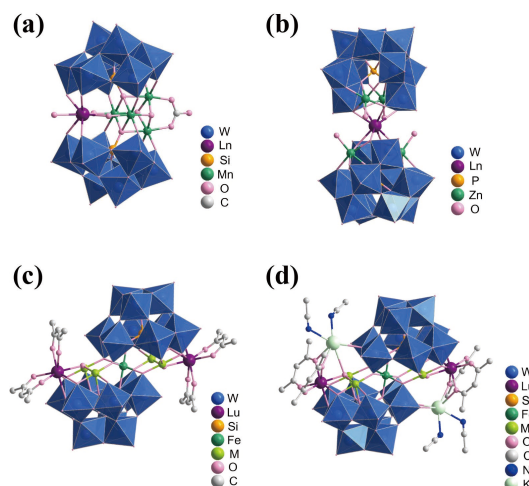tion between different metal ions and POMs makes the synthesis of POM-based 3d–4f clusters particularly difficult. We summarize the following strategies for the synthesis of POM-based LnOCs in the literature.

3.1 Lacunary POM-based ligand-directed method

This method uses lacunary POMs as the reaction material and the ligand-directing effect of O to obtain POM-based LnOCs. Many synthetic methods were reported in the literature for the synthesis of different types of lacunary POMs, and most of them are simple and have high yields. More importantly, it is easier to adjust the reaction ratio between ligands and metal ions using lacunary POMs as the direct reaction material, facilitating the success of the synthesis and atomic utilization. Thus, the use of lacunary POMs as a precursor is a common and efficient synthesis method. Nearly half of the POM-based LnOCs in the literature have been synthesized by this method, especially POM-based pure 4f clusters (Table 1). In this synthesis method, trilacunary POMs are more common, including Keggin POMs [GeW$_9$], [SiW$_9$], [AsW$_9$], and [SbW$_9$], and Dawson POM [P$_2$W$_{15}$]. These lacunary POMs have a strong nucleophilic ability, and the O in their absence is a clear coordination site, which provides a coordinated-guiding effect to form 3:2 and 4:2 sandwich-type clusters, as well as clusters with [POMLn$_3$] and [POMLnM$_3$] as assembly units. For example, a series of POM-based pure 4f clusters with [Ce$_6$] as the assembly unit obtained from the trilacunary POM [AsW$_9$] were introduced previously, the giant POM-based 3d–4f clusters [{(GeW$_9$O$_{34}$)$_2$Ln$_3$(H$_2$O)(OH)$_3$}$_6${M$_2$Ln$_3$(μ$_3$-OH)$_6$(OH$_2$)$_6$}$_4$]$^{56-}$ from trilacunary POMs [GeW$_9$] and the POM-based 3d–4f cluster {[LnNi$_3$(OH)$_3$(B-α-SiW$_9$O$_{34}$)]$_4$B$_{22}$O$_{42}$}$^{34-}$ from trilacunary POMs [SiW$_9$].

3.2 *In-situ* transformation of lacunary POMs ligand-directed method

Due to the high sensitivity of the structures of POMs to pH and other reaction environments, novel structural clusters can be obtained by their further decomposition or reconstruction in response to changes in the reaction environment during the reaction. In addition, it offers the advantage of the lacunary POM-based ligand-directed method. Currently, more than half of the LnOCs were synthesized using this method in the literature, especially 5d–4f and 5p–4f clusters with novel structures. The transformation characteristics of some lacunary POMs have been initially studied. For example, [As$_2$W$_{19}$O$_{67}$(H$_2$O)] is prone to the shedding of [WO$_5$(H$_2$O)] units to form trilacunary POMs [AsW$_9$] and tetralacunary POMs [AsW$_8$]. Moreover, the trilacunary POM [B-α-SbW$_9$] is susceptible to configurational conversion to form [B-β-SbW$_9$]. The transformation of heteroatoms occurs to obtain trilacunary [B-α-PW$_9$]. Notably, it can even form trilacunary [B-α-NiW$_9$] and [B-α-FeW$_9$] containing 3d heteroatoms, which is of great significance for enriching the topology of POM-based clusters. For now, we cannot fully grasp the transition rules of these metastable POMs, whose influence factors are not only limited to the solution pH.

3.3 *In-situ* generation of lacunary POMs ligand-directed method

This method refers to the synthesis of POM-based LnOCs by the

direct one-pot reaction with lanthanide ions using simple raw materials required for the synthesis of lacunary POMs (also known as the "one-pot method"). This synthesis method is characterized by the simplicity of the synthesis steps, as well as the ease of obtaining some unique assembly units involved in the synthesis during the reaction, especially some tungstate structures; thus, it was mainly used for the synthesis of POM-based 5d–4f clusters (Table 2). This method also has poor designability and low predictability due to the complexity of raw materials and the influential factors in the *in-situ* synthesis of lacunary POMs.

3.4 Mixed synthesis strategies

Mixed synthesis strategies have been shown to be effective to prepare POM-based LnOCs. For example, inorganic anions such as CO_3^{2-}, WO_4^{2-}, and PO_4^{3-} can act as the anionic template in the synthesis of POM-based LnOCs. The cluster Ln_3Ni_2 was obtained based on the lacunary POM-based ligand-directed method by adding the templating anion CO_3^{2-}, while the cluster Ln_3Ni_9 was obtained by templating PO_4^{3-} in which PO_4^{3-} replaced SbO_3^{3-} *in-situ* to generate the trilacunary POM $[PW_9]$ with $[SbW_9]$ to participate in the structural assembly. The lacunary POMs $[PW_9]$ and $[SbW_9]$ have completely different coordination modes because of the differences between PO_4^{3-} and SbO_3^{3-}. The cluster Ln_3Ni_9 is a rare example of the POM-based 3d–4f clusters obtained by the *in-situ* transformation of lacunary POMs ligand-directed method and is the first POM-based 3d–4f cluster containing mixed lacunary POMs (Fig. 19).

Based on the slow-release strategy of lanthanide ions, the largest POM-based 3d–4f cluster $La_{10}Ni_{48}$ and the first POM-based 3d–4f cluster containing 3d heteroatom Fe_4Ln_2 (Fig. 20) were obtained. Previous studies usually used rare earth oxides in strongly acidic nitric acid solutions. Under weakly acidic conditions, rare earth oxides can slowly release Ln^{3+} ions. The target products can be obtained by adding different insoluble rare earth compounds, including rare earth oxides, hydroxides, and sulfates, but the target products cannot be obtained by adding soluble rare earth salts. The use of insoluble rare earth compounds effectively overcomes the strong reaction of rare earth ions with POMs and provides easy precipitation, which facilitates the crystallization of POM-based LnOCs and improves atomic utilization [133, 134, 143]. A class of trimeric clusters, $\{(WO_4)[Ln(H_2O)(Ac)(B\text{-}\alpha\text{-}SbW_9O_{31}(OH)_2)]_3\}^{17-}$ (Ln = Eu, Dy, Ho, and Gd), can be regarded as three trilacunary POMs $[SbW_9]$ and three OAc^- co-coordinated with three Ln^{3+}, and $[WO_4]^{2-}$ in a tetrahedral configuration acts as an anionic template for the formation of these LnOCs. The inorganic anion $[HPO_3]^{2-}$ has a similar structure-directing role as $[WO_4]^{2-}$, as shown in the cluster $\{[Ln_3(CH_3COO)_3(HPO_3)(WO_4)][B\text{-}\alpha\text{-}SbW_9O_{33}]_3\}^{25-}$ (Ln = Eu, Tb, Dy, Ho, and Er) [158–159]. In addition, the addition of organic solubilizers can improve the reactivity of Ln ions to a certain extent [140–147].

4 Applications of POM-based LnOCs

POMs have multiple structural tunability in terms of elemental composition, atomic number, counterions, valence state, and backbone structure, and are therefore easily designed for functionalization. POMs have applications in electronics, electrochemistry, catalysis, biology, nanomaterials, and surface science. POM-based LnOCs offer unique optical and magnetic properties owing to lanthanide ions and have applications in

catalysis, proton conduction, biomedicine, electrochemistry, and other related fields [52, 56, 58, 76, 88, 153, 157]. In this review, we focus on the properties of POM-based LnOCs relevant to single-molecule magnets and proton conductivity.

4.1 Single-molecule magnets

Single-molecule magnets (SMMs) have potential applications in high-density information storage, magnetic quantum dots, and spintronic devices. The magnetization reversal barrier (U_{eff}) and the magnetic blocking temperature (T_B) are two key indicators to judge the performance of SMMs, and higher U_{eff} and T_B indicate better SMM performance. LnOCs with large anisotropy are potential SMMs [160]. Lacunary POMs not only provide a well-defined and rigid coordination environment but also facilitate magnetic isolation due to their large size and the presence of antibalance ions and solvents between them. In addition, they induce strong axial magnetic anisotropy, making them an ideal inorganic ligand for SMMs [55, 83, 85, 161, 162].

Since Gaita-Ariño reported the first SMM $[ErW_{10}O_{36}]^{9-}$ in 2008 [163], POM-based LnOCs-type SMMs including pure 4f clusters, 5d–4f clusters, and 3d–4f clusters have been studied. As shown in Table 4, the U_{eff} of most POM-based LnOCs are currently less than 100 K. $\{[(AsW_9O_{33})_3Dy_2(H_2O)_4W_4O_9(H_2O)]_2[NH_2(CH_2PO_3)_2]\}^{33-}$ has a breakthrough U_{eff} value of 101 K under zero applied field, which is the maximum value reported for POM-based LnOCs [87]. Among the clusters $[(PW_{11}O_{39})_2Dy_2X_2(H_2O)_2]^{10-}$ (X = OH(1), F(2), and OAc(3)), compounds 1 and 3 exhibit antiferromagnetic interactions, cluster 2 exhibits ferromagnetic interactions, and effective magnetic isolation is achieved between adjacent molecules in all three clusters. Clusters 1 and 2 act as SMMs at zero direct current (DC) field, while cluster 3 does not. Cluster 1 has an energy barrier of 98 cm^{-1} at zero field, which is the highest effective energy barrier for magnetization reversal among the POM-based SMMs. This indicates that the bridging ligand affects not only the magnetic coupling interaction between Dy^{3+} and the arrangement of the main magnetic axis but also the behavior of SMMs [55]. The cluster $[FeMn_4\{Lu(L)_2\}_2O_2(A\text{-}\alpha\text{-}SiW_9O_{34})_2]$ reported by Mizuno showed the performance of SMMs under zero field with a U_{eff} value of 19.7 K. They then used an automated platform to obtain the clusters $[FeMn_4\{Lu(L)_2A\}_2O_2(A\text{-}\alpha\text{-}SiW_9O_{34})_2]$ (A = Ag, Na, and K; L = acetylacetonate) in a predicted multistep reaction. When A = Ag and Na, its U_{eff} vale doubled. The results offer a good model for the study of magnetic coupling and SMM properties [144, 145].

4.2 Proton-conducting materials

Proton-conducting materials can be used as electrolytes for fuel cells, gas sensors, and other electrochemical devices, and proton conduction in solids has attracted a lot of attention in materials chemistry. POMs are potential proton-conducting materials owing to their low effective surface charge density, high thermal stability, abundant proton carriers, discrete mobile ion composition, and pseudoliquid phase behavior. At the same time, structure-defined POM crystal materials provide an opportunity to study proton conduction pathways and mechanisms and offer theoretical guidance for the synthesis of new proton-conducting materials [27–29]. The excellent proton-conducting properties of the heteropolyacid $H_3PMo_{12}O_{40}$ were discovered in 1979 [164]. To date, various forms of POM-based materials have been studied as proton-conducting materials. The introduction of the Lewis acid center can become new proton donors, and POMs can be used as proton

Table 4 Comparison of U_{eff} values for POMs-based LnOCs

LnOCs	U_{eff}/k_B	DC field (Oe)
$[\text{ErW}_{10}\text{O}_{36}]^{9-}$ [163]	55.2 K	Zero
$[\{\text{Dy}(\text{H}_2\text{O})_2(\alpha_2\text{-As}_2\text{W}_{17}\text{O}_{61})\}_2]^{14-}$ [54]	11.8 K	1000
$[\text{Dy}_4\text{As}_5\text{W}_{40}\text{O}_{144}(\text{H}_2\text{O})_{10}(\text{Gly})_2]^{21-}$ [90]	3.9 K	10
$[\text{Dy}(\text{C}_4\text{H}_2\text{O}_6)(\alpha\text{-PW}_{11}\text{O}_{39})]_2^{16-}$ [58]	20 K	4000
$[\text{FeMn}_4\{\text{Lu}(\text{L})_2\}_2\text{O}_2(\text{A-}\alpha\text{-SiW}_9\text{O}_{34})_2]$ [144]	19.7 K	Zero
$[\text{FeM}_4\{\text{Lu}(\text{L})_2\text{Ag}\}_2\text{O}_2(\text{A-}\alpha\text{-SiW}_9\text{O}_{34})_2]$ [144]	40.0 K	Zero
$[\text{FeM}_4\{\text{Lu}(\text{L})_2\text{Na}\}_2\text{O}_2(\text{A-}\alpha\text{-SiW}_9\text{O}_{34})_2]$ [144]	40.3 K	Zero
$[\text{FeM}_4\{\text{Lu}(\text{L})_2\text{K}\}_2\text{O}_2(\text{A-}\alpha\text{-SiW}_9\text{O}_{34})_2]$ [144]	26.7 K	Zero
$[\{(\text{AsW}_9\text{O}_{33})\text{Dy}(\text{H}_2\text{O})_2\}_6]^{36-}$ [83]	68 K	3000
$[\{(\text{AsW}_9\text{O}_{33})_3\text{Dy}_2(\text{H}_2\text{O})_4\text{W}_4\text{O}_9(\text{H}_2\text{O})\}_2$ $(\text{NH}_2(\text{CH}_2\text{PO}_3)_2)]^{33-}$ [87]	101 K	Zero
$[\{(\text{AsW}_9\text{O}_{33})_3\text{Dy}_2(\text{H}_2\text{O})_4\text{W}_4\text{O}_9(\text{H}_2\text{O})\}_2$ $(\text{NH}_2(\text{CH}_2\text{PO}_3)_2)]^{33-}$ [87]	158 K	5000
$[\{\text{Dy}(\text{H}_2\text{O})(\text{Hpic})_3][\text{Dy}(\text{Hpic})_2$ $(\alpha_2\text{-P}_2\text{W}_{17}\text{O}_{61})]\}]^{4-}$ [60]	119.38 K	4000
$[\text{Dy}_9(\text{CO}_3)_3(\text{ampH})_2(\text{H}_2\text{O})_{12}(\text{PW}_{10}\text{O}_{37})_6]^{35-}$ [79]	56 K	Zero
$[(\text{PW}_{11}\text{O}_{39})_2\text{Dy}(\text{OH})_2(\text{H}_2\text{O})_2]^{10-}$ [55]	98 cm^{-1}	Zero
$[(\text{PW}_{11}\text{O}_{39})_2\text{Dy}_2(\text{F})_2(\text{H}_2\text{O})_2]^{10-}$ [55]	74 cm^{-1}	Zero
$[\text{Gd}\{\text{Zn}_2\text{PW}_{10}\text{O}_{38}(\text{H}_2\text{O})_2\}_2]^{11-}$ [141]	6.30 K	1000
$[\text{Tb}\{\text{Zn}_2\text{PW}_{10}\text{O}_{38}(\text{H}_2\text{O})_2\}_2]^{11-}$ [141]	4.54 K	1000
$[\text{Er}\{\text{Zn}_2\text{PW}_{10}\text{O}_{38}(\text{H}_2\text{O})_2\}_2]^{11-}$ [141]	9.08 K	1000
$[\text{Yb}\{\text{Zn}_2\text{PW}_{10}\text{O}_{38}(\text{H}_2\text{O})_2\}_2]^{11-}$ [141]	10.7 K	1000
$[\text{Dy}(\alpha\text{-PW}_{11}\text{O}_{39})_2]^{11-}$ [93]	55 K	3000
$[\{\text{Dy}(\alpha\text{-PW}_{11}\text{O}_{39})(\text{H}_2\text{O})_3\}_2]^{8-}$ [93]	57 K	3000
$[(\text{DyOH})_3(\text{CO}_3)(\alpha\text{-PW}_9\text{O}_{34})_2]^{11-}$ [93]	37 K	3000
$[\text{Dy}_8(\text{PW}_{10}\text{O}_{38})_4(\text{OH})_4(\text{H}_2\text{O})_2(\text{W}_3\text{O}_{14})]^{26-}$ [93]	64 K	3000
$[\text{Er}(\beta_2\text{-GeW}_{11}\text{O}_{39})(\alpha\text{-GeW}_{11}\text{O}_{39})]^{13-}$ [50]	43.3 cm^{-1}	500
$[\text{Co}(\text{H}_2\text{O})\text{Dy}_3(\text{H}_2\text{O})_5(\text{W}_3\text{O}_{11})(\text{SbW}_9\text{O}_{33})_3]^{20-}$ [150]	9.0 K	2500
$[\text{Ni}(\text{H}_2\text{O})\text{Dy}_3(\text{H}_2\text{O})_5(\text{W}_3\text{O}_{11})(\text{SbW}_9\text{O}_{33})_3]^{20-}$ [150]	6.5 K	2000
$[\text{Fe}_2\text{Dy}_2(\text{H}_2\text{O})_4(\text{B-}\alpha\text{-FeW}_9\text{O}_{34})_2]^{10-}$ [143]	50.24 K	Zero
$[\text{Fe}_2\text{Dy}_2(\text{H}_2\text{O})_4(\text{B-}\alpha\text{-FeW}_9\text{O}_{34})_2]^{10-}$ [143]	80.21 K	2500

acceptors, improving proton conductivity [29]. In 2016, the Niu group reported a two-dimensional (2D) graphite-like framework with a POM-based pure 4f cluster $\{[\text{Ce}^{IV}_7\text{Ce}^{III}_3\text{O}_6(\text{OH})_6(\text{CO}_3)(\text{H}_2\text{O})_{11}][(\text{P}_2\text{W}_{16}\text{O}_{59})]_3\}^{19-}$ as nodes, and its proton conductivity reached 2.65×10^{-4} S·cm^{-1} at 98% RH of 100 °C with an activation energy of 0.36 eV [80]. The Zheng group found that the conductivity of the cluster $[\text{La}_{27}\text{Ge}_{10}\text{W}_{106}\text{O}_{406}(\text{OH})_4(\text{H}_2\text{O})_{24}]^{59-}$ was up to 1.5×10^{-2} S·cm^{-1} at 98% RH of 85 °C [96]. They also reported the proton conductivity of other POM-based LnOCs. Among them, the conductivity of the cluster $[\text{Sc}_4(\text{C}_2\text{O}_4)_4(\text{B-}\beta\text{-SbW}_9\text{O}_{33})_2][\text{Sc}_4(\text{H}_2\text{O})_2(\text{C}_2\text{O}_4)4(\text{B-}\beta\text{-SbW}_9\text{O}_{33})_2]^{28-}$ was 7.9×10^{-4} S·cm^{-1} at 98% RH and 25 °C with an activation energy of 0.28 eV [74]. The conductivity of the cluster $\{[\text{Gd}_2(\text{H}_2\text{O})_{11}]_2[\text{Gd}_3(\text{H}_2\text{O})_3(\alpha\text{-SiW}_{11}\text{O}_{39})_2]_2\}^{2-}$ was 3.54×10^{-3} S·cm^{-1} at 98% RH and 85 °C with an activation energy of 0.38 eV [97]. Another cluster, $\{\text{La}_{10}(\mu_3\text{-OH})_2(\text{H}_2\text{O})_{10}[\alpha(1,8)\text{-GeW}_{10}\text{O}_{38}]_2[\beta(4,11)\text{-GeW}_{10}\text{O}_{38}]_2\}^{20-}$, showed a conductivity of 6.35×10^{-4} S·cm^{-1} at 98%

RH and 85 °C with an activation energy of 0.49 eV [82]. $\{[\text{W}_{14}\text{Ce}^{IV}_6\text{O}_{61}][(\text{W}_3\text{Bi}_6\text{Ce}^{III}_3(\text{H}_2\text{O})_3\text{O}_{14})(\text{B-}a\text{-BiW}_9\text{O}_{33})_3]_2\}^{34-}$ had a conductivity of 4.9×10^{-7} S·cm^{-1} at −40 °C, which is the first report on the proton conductivity of POM-based materials in nonaqueous environments below 0 °C [165]. The conductivity of $[\text{La}_{10}\text{Ni}_{48}\text{W}_{140}\text{Sb}_{16}\text{P}_{12}\text{O}_{568}(\text{OH})_{24}(\text{H}_2\text{O})_{20}]^{86-}$ reached 2.05×10^{-2} S·cm^{-1} at 100% RH at 22 °C with an activation energy of 0.22 eV [134]. In general, some POM-based LnOCs with excellent proton conductivities have been developed (Table 5), but they are still far from being used in practical applications due to hygroscopicity and the tendency to lose water molecules at high temperatures. The design and synthesis of POM-based LnOCs with humidity resistance and heat stability remain challenging [28].

5 Summary and outlook

POM-based LnOCs have received considerable attention owing to their interesting structures and potential applications. Various POM-based LnOCs with a rich variety of structures and interesting properties have been reported, especially pure 4f clusters, 5d–4f clusters, and 3d–4f clusters, as well as 4s–4f clusters, 4p–4f clusters, 5p–4f clusters, and 5p–5d–4f clusters. Several effective synthesis methods of POM-based LnOCs have also been developed. For example, the lacunary POM-based ligand-directed method utilizes the added precursor lacunary POMs to be directly involved in the structural assembly. For the *in-situ* transformation of lacunary POMs ligand-directed method, the added precursor lacunary POMs are first converted into new lacunary POMs *in-situ* and then involved in the structural assembly. The *in-situ* generation of lacunary POMs ligand-directed method is also known as the one-pot method, which uses raw materials that participate in the reaction. The first two synthesis strategies require the synthesis of lacunary POMs but are more conducive to the regulation of the ratio of reaction materials. The easy hydrolysis of Ln ions and the strong reactivity between Ln and POMs leading to easy precipitation and difficult crystallization, coupled with the coordination competition between different metal ions and POMs, make the synthesis of POM-based LnOCs difficult, especially high-nuclearity clusters. A mixed strategy involving the organic auxiliary ligand method, anionic template methods, and the slow-release strategy of lanthanide ions may be the most effective method for the synthesis of POM-based LnOCs. More importantly, the development of interdisciplinary approaches such as the application of artificial intelligence to the synthesis of POM-based LnOCs offers an exciting research direction, which is beneficial to not only the study of the assembly mechanism but also the industrialization of its applications.

POM-based LnOCs offer potential applications owing to not only the interesting properties of POMs in the fields of magnetism, electronics, electrochemistry, catalysis, optics, and biology but also the unique advantages of lanthanide clusters in magneto-optics. In addition to the application characteristics of POMs and lanthanide ions, the synergistic effect between them may offer great application potential. However, the applications of POM-based LnOCs have not been extensively studied so far, mainly in the areas of magnetic and proton conduction. Although various POM-based LnOCs with SMM properties have been reported, their U_{eff} and T_B could be improved compared to organic ligand LnOCs. Meanwhile, some POM-based LnOCs with excellent proton conductivities have been reported, but issues such as hygroscopicity and easy dehydration at

Table 5 Comparison of the proton conductivity in some representative POM-based LnOCs[a]

Compounds	σ (S·cm^{-1}) (°C, RH)	E_a (eV)
$[La_{10}Ni_{48}W_{140}Sb_{16}P_{12}O_{568}(OH)_{24}(H_2O)_{20}]^{86-}$ [134]	2.05×10^{-2} (22 °C, 100%)	0.22/58%
	3.74×10^{-3} (22 °C, 88%)	
	6.86×10^{-4} (22 °C, 72%)	
	3.28×10^{-4} (22 °C, 65%)	
	3.09×10^{-4} (22 °C, 58%)	
	3.25×10^{-4} (25 °C, 58%)	
	3.57×10^{-4} (30 °C, 58%)	
	3.92×10^{-4} (35 °C, 58%)	
	4.45×10^{-4} (40 °C, 58%)	
	4.89×10^{-4} (45 °C, 58%)	
$[La_{27}Ge_{10}W_{106}O_{406}(OH)_4(H_2O)_{24}]^{59-}$ [96]	1.5×10^{-2} (85 °C, 98%)	0.42/98%
	1.8×10^{-3} (30 °C, 98%)	
	3.8×10^{-4} (30 °C, 55%)	
	1.5×10^{-2} (85 °C, 98%)	
$\{[Ce^{IV}_7Ce^{III}_3O_6(OH)_6(CO_3)(H_2O)_{11}][(P_2W_{16}O_{59})]_3\}^{19-}$ [80]	2.65×10^{-4} (100 °C, 98%)	0.36/98%
	1.95×10^{-7} (30 °C, 98%)	
$\{[W_{14}Ce^{IV}_6O_{61}]([W_3Bi_6Ce^{III}_3(H_2O)_3O_{14}][B\text{-}\alpha\text{-}BiW_9O_{33}]_3)_2\}^{34-}$ [165]	2.4×10^{-3} (25 °C, 90%)	0.677/—
	2.6×10^{-4} (25 °C, 50%)	Anhydrous
	4.9×10^{-7} (−40 °C)	
$[Sc_4(C_2O_4)_4(B\text{-}\beta\text{-}SbW_9O_{33})_2][Sc_4(H_2O)_2(C_2O_4)_4(B\text{-}\beta\text{-}SbW_9O_{33})_2]^{28-}$ [74]	3.1×10^{-2} (75 °C, 98%)	0.28/98%
	7.9×10^{-4} (25 °C, 98%)	
	3.0×10^{-4} (25 °C, 55%)	
$\{[Gd_2(H_2O)_{11}]_2[Gd_3(H_2O)_3(\alpha\text{-}SiW_{11}O_{39})_2]_2\}^{2-}$ [97]	3.54×10^{-3} (85 °C, 98%)	0.38/98%
	1.56×10^{-4} (25 °C, 98%)	
$\{La_{10}(\mu_3\text{-}OH)_2(H_2O)_{10}[\alpha(1,8)\text{-}GeW_{10}O_{38}]_2[\beta(4,11)\text{-}GeW_{10}O_{38}]_2\}^{20-}$ [82]	6.35×10^{-4} (85 °C, 98%)	0.49/98%
	4.68×10^{-5} (30 °C, 98%)	
	8.66×10^{-7} (30 °C, 55%)	

[a] σ: proton conductivity, E_a: proton transport activation energy, and RH: relative humidity.

high temperatures must be addressed for practical applications. The development of POM-based LnOCs is mainly limited by the difficulty of their synthesis. Developing effective synthesis strategies and exploring the functionalization of LnOCs to realize the applications of POM-based lanthanide clusters will be strategic research directions in this field.

Acknowledgements

Declaration of competing interest

The authors have no competing interests to declare that are relevant to the content of this article.

Author contribution statement

The manuscript was written through contributions of all authors.

References

[1] Guo, F. S.; Day, B. M.; Chen, Y. C.; Tong, M. L.; Mansikkamäki, A.; Layfield, R. A. Magnetic hysteresis up to 80 kelvin in a dysprosium metallocene single-molecule magnet. *Science* **2018**, *362*, 1400–1403.

[2] Fu, X.; Fu, S.; Lu, Q.; Zhang, J.; Wan, P. P.; Liu, J. L.; Zhang, Y.; Chen, C. H.; Li, W.; Wang, H. D. et al. Excitation energy mediated cross-relaxation for tunable upconversion luminescence from a single lanthanide ion. *Nat. Commun.* **2022**, *13*, 4741.

[3] Xu, Q. F.; Liu, B. L.; Ye, M. Y.; Zhuang, G. L.; Long, L. S.; Zheng, L. S. Gd(OH)F$_2$: A promising cryogenic magnetic refrigerant. *J. Am. Chem. Soc.* **2022**, *144*, 13787–13793.

[4] Schroll, C. A.; Chatterjee, S.; Levitskaia, T. G.; Heineman, W. R.; Bryan, S. A. Electrochemistry and Spectroelectrochemistry of Europium (III) Chloride in 3LiCl-2KCl from 643 to 1123 K. *Anal. Chem.* **2013**, *85*, 9924–9931.

[5] Li, X. Z.; Tian, C. B.; Sun, Q. F. Coordination-directed self-assembly of functional polynuclear lanthanide supramolecular architectures. *Chem. Rev.* **2022**, *122*, 6374–6458.

[6] Sahoo, S.; Mondal, S.; Sarma, D. Luminescent lanthanide metal organic frameworks (LnMOFs): A versatile platform towards organomolecule sensing. *Coord. Chem. Rev.* **2022**, *470*, 214707.

[7] Chen, R.; Chen, C. L.; Du, M. H.; Wang, X.; Wang, C.; Long, L. S.; Kong, X. J.; Zheng, L. S. Soluble lanthanide-transition-metal clusters Ln$_{36}$Co$_{12}$ as effective molecular electrocatalysts for water oxidation. *Chem. Commun. (Camb.)* **2021**, *57*, 3611–3614.

[8] Du, M. H.; Chen, L. Q.; Jiang, L. P.; Liu, W. D.; Long, L. S.; Zheng, L. S.; Kong, X. J. Counterintuitive lanthanide hydrolysis-induced

assembly mechanism. *J. Am. Chem. Soc.* **2022**, *144*, 5653–5660.

[9] Du, M. H.; Wang, D. H.; Wu, L. W.; Jiang, L. P.; Li, J. P.; Long, L. S.; Zheng, L. S.; Kong, X. J. Hierarchical assembly of coordination macromolecules with atypical geometries: $Gd_{44}Co_{28}$ crown and $Gd_{95}Co_{60}$ cage. *Angew. Chem., Int. Ed.* **2022**, *61*, e202200537.

[10] Liu, W. D.; Li, G. J.; Xu, H.; Du, M. H.; Long, L. S.; Zheng, L. S.; Kong, X. J. Photoluminescence of lanthanide-titanium-oxo clusters Eu_9Ti_2 and Tb_9Ti_2 based on a *β*-diketone ligand. *Inorg. Chem.* **2022**, *61*, 9849–9854.

[11] Wang, X.; Wang, S. Q.; Chen, J. N.; Jia, J. H.; Wang, C.; Paillot, K.; Breslavetz, I.; Long, L. S.; Zheng, L. S.; Rikken, G. L. J. A. et al. Magnetic 3d-4f chiral clusters showing multimetal site magneto-chiral dichroism. *J. Am. Chem. Soc.* **2022**, *144*, 8837–8847.

[12] Weng, Z. Z.; Xie, J.; Huang, K. X.; Li, J. P.; Long, L. S.; Kong, X. J.; Zheng, L. S. Asymmetric cyanosilylation of aldehydes by a lewis acid/base synergistic catalyst of chiral metal clusters. *Inorg. Chem.* **2022**, *61*, 4121–4129.

[13] Chen, R.; Hong, Z. F.; Zhao, Y. R.; Zheng, H.; Li, G. J.; Zhang, Q. C.; Kong, X. J.; Long, L. S.; Zheng, L. S. Ligand-dependent luminescence properties of lanthanide-titanium oxo clusters. *Inorg. Chem.* **2019**, *58*, 15008–15012.

[14] Chen, R.; Yan, Z. H.; Kong, X. J.; Long, L. S.; Zheng, L. S. Integration of lanthanide-transition-metal clusters onto CdS surfaces for photocatalytic hydrogen evolution. *Angew. Chem., Int. Ed.* **2018**, *57*, 16796–16800.

[15] Chen, R.; Zhuang, G. L.; Wang, Z. Y.; Gao, Y. J.; Li, Z.; Wang, C.; Zhou, Y.; Du, M. H.; Zeng, S. Y.; Long, L. S. et al. Integration of bio-inspired lanthanide-transition metal cluster and P-doped carbon nitride for efficient photocatalytic overall water splitting. *Natl. Sci. Rev.* **2021**, *8*, nwaa234.

[16] Jin, P. B.; Yu, K. X.; Luo, Q. C.; Liu, Y. Y.; Zhai, Y. Q.; Zheng, Y. Z. Tetraanionic arachno-carboranyl ligand imparts strong axiality to terbium(III) single-molecule magnets. *Angew. Chem., Int. Ed.* **2022**, *61*, e202203285.

[17] Zhang, H. L.; Zhai, Y. Q.; Nojiri, H.; Schröder, C.; Hsu, H. K.; Chan, Y. T.; Fu, Z. D.; Zheng, Y. Z. {Sc_nGd_n} heterometallic rings: Tunable ring topology for spin-wave excitations. *J. Am. Chem. Soc.* **2022**, *144*, 15193–15202.

[18] Chen, S. S.; Su, H. F.; Long, L. S.; Zheng, L. S.; Kong, X. J. Hydrolysis-promoted building block assembly: Structure transformation from Y_{12} wheel and Y_{34} ship to Y_{60} cage. *Inorg. Chem.* **2021**, *60*, 16922–16926.

[19] Du, M. H.; Xu, S. H.; Li, G. J.; Xu, H.; Lin, Y.; Liu, W. D.; Long, L. S.; Zheng, L. S.; Kong, X. J. Modification of multi-component building blocks for assembling giant chiral lanthanide-titanium molecular rings. *Angew. Chem., Int. Ed.* **2022**, *61*, e202116296.

[20] Huang, W. M.; Chen, W. M.; Bai, Q. X.; Zhang, Z.; Feng, M.; Zheng, Z. P. Anion-guided stepwise assembly of high-nuclearity lanthanide hydroxide clusters. *Angew. Chem., Int. Ed.* **2022**, *61*, e202205385.

[21] Pan, Z. H.; Weng, Z. Z.; Kong, X. J.; Long, L. S.; Zheng, L. S. Lanthanide-containing clusters for catalytic water splitting and CO_2 conversion. *Coord. Chem. Rev.* **2022**, *457*, 214419.

[22] Zheng, X. Y.; Kong, X. J.; Zheng, Z. P.; Long, L. S.; Zheng, L. S. High-nuclearity lanthanide-containing clusters as potential molecular magnetic coolers. *Acc. Chem. Res.* **2018**, *51*, 517–525.

[23] Zheng, X. Y.; Xie, J.; Kong, X. J.; Long, L. S.; Zheng, L. S. Recent advances in the assembly of high-nuclearity lanthanide clusters. *Coord. Chem. Rev.* **2019**, *378*, 222–236.

[24] Das, V.; Kaushik, R.; Hussain, F. Heterometallic 3*d*-4*f* polyoxometalates: An emerging field with structural diversity to multiple applications. *Coord. Chem. Rev.* **2020**, *413*, 213271.

[25] Fang, X. K.; Kögerler, P.; Speldrich, M.; Schilder, H.; Luban, M. A polyoxometalate-based single-molecule magnet with an $S = 21/2$ ground state. *Chem. Commun. (Camb.)* **2012**, *48*, 1218–1220.

[26] Ma, X.; Yang, W.; Chen, L. J.; Zhao, J. W. Significant developments in rare-earth-containing polyoxometalate chemistry: Synthetic strategies, structural diversities and correlative properties. *CrystEngComm* **2015**, *17*, 8175–8197.

[27] Meng, X.; Wang, H. N.; Song, S. Y.; Zhang, H. J. Proton-conducting crystalline porous materials. *Chem. Soc. Rev.* **2017**, *46*, 464–480.

[28] Ogiwara, N.; Iwano, T.; Ito, T.; Uchida, S. Proton conduction in ionic crystals based on polyoxometalates. *Coord. Chem. Rev.* **2022**, *462*, 214524.

[29] Yang, P.; Alsufyani, M.; Emwas, A. H.; Chen, C. Q.; Khashab, N. M. Lewis acid guests in a {P_8W_{48}} archetypal polyoxotungstate host: Enhanced proton conductivity via metal-oxo cluster within cluster assemblies. *Angew. Chem., Int. Ed.* **2018**, *57*, 13046–13051.

[30] Boskovic, C. Rare earth polyoxometalates. *Acc. Chem. Res.* **2017**, *50*, 2205–2214.

[31] Wang, Z. M.; Xin, X.; Zhang, M.; Li, Z.; Lv, H. J.; Yang, G. Y. Recent advances of mixed-transition-metal-substituted polyoxometalates. *Sci. China Chem.* **2022**, *65*, 1515–1525.

[32] Liu, J. C.; Zhao, J. W.; Streb, C.; Song, Y. F. Recent advances on high-nuclear polyoxometalate clusters. *Coord. Chem. Rev.* **2022**, *471*, 214734.

[33] Zhao, J. W.; Li, Y. Z.; Chen, L. J.; Yang, G. Y. Research progress on polyoxometalate-based transition-metal-rare-earth heterometallic derived materials: Synthetic strategies, structural overview and functional applications. *Chem. Commun. (Camb.)* **2016**, *52*, 4418–4445.

[34] Bijelic, A.; Aureliano, M.; Rompel, A. Polyoxometalates as potential next-generation metallodrugs in the combat against cancer. *Angew. Chem., Int. Ed.* **2019**, *58*, 2980–2999.

[35] Chen, X. L.; Zhou, Y.; Roy, V. A. L.; Han, S. T. Evolutionary metal oxide clusters for novel applications: Toward high-density data storage in nonvolatile memories. *Adv. Mater.* **2018**, *30*, 1703950.

[36] Liu, J. X.; Zhang, X. B.; Li, Y. L.; Huang, S. L.; Yang, G. Y. Polyoxometalate functionalized architectures. *Coord. Chem. Rev.* **2020**, *414*, 213260.

[37] Sun, M.; Zhang, J. Z.; Putaj, P.; Caps, V.; Lefebvre, F.; Pelletier, J.; Basset, J. M. Catalytic oxidation of light alkanes (C_1-C_4) by heteropoly compounds. *Chem. Rev.* **2014**, *114*, 981–1019.

[38] Yang, L.; Lei, J.; Fan, J. M.; Yuan, R. M.; Zheng, M. S.; Chen, J. J.; Dong, Q. F. The intrinsic charge carrier behaviors and applications of polyoxometalate clusters based materials. *Adv. Mater.* **2021**, *33*, 2005019.

[39] Zhang, M.; Li, H. J.; Zhang, J. H.; Lv, H. J.; Yang, G. Y. Research advances of light-driven hydrogen evolution using polyoxometalate-based catalysts. *Chin. J. Catal.* **2021**, *42*, 855–871.

[40] Zhao, H. Y.; Li, Y. Z.; Zhao, J. W.; Wang, L.; Yang, G. Y. State-of-the-art advances in the structural diversities and catalytic applications of polyoxoniobate-based materials. *Coord. Chem. Rev.* **2021**, *443*, 213966.

[41] Peacock, R. D.; Weakley, T. J. R. Heteropolytungstate complexes of the lanthanide elements. Part I. Preparation and reactions. *J. Chem. Soc. A* **1971**, 1836–1839

[42] Peacock, R. D.; Weakley, T. J. R. Heteropolytungstate complexes of the lanthanide elements. Part Ⅱ. Electronic spectra:A metal-ligand charge-transfer transition of cerium (Ⅲ). *J. Chem. Soc. A* **1971**, 1937–1940

[43] Lin, Y. D.; Ge, R.; Tian, C. B.; Sun, C.; Sun, Y. Q.; Zeng, Q. X.; Li, X. X.; Zheng, S. T. 3d-4f Heterometallic cluster incorporated polyoxoniobates with magnetic properties. *Chem. Commun. (Camb.)* **2021**, *57*, 8624–8627.

[44] Ribó, E. G.; Bell, N. L.; Long, D. L.; Cronin, L. Engineering highly reduced molybdenum polyoxometalates via the incorporation of d and f block metal ions. *Angew. Chem., Int. Ed.* **2022**, *61*, e202201672.

[45] Jin, L.; Li, X. X.; Qi, Y. J.; Niu, P. P.; Zheng, S. T. Giant hollow

heterometallic polyoxoniobates with sodalite-type lanthanide-tungsten-oxide cages: Discrete nanoclusters and extended frameworks. *Angew. Chem., Int. Ed.* **2016**, *55*, 13793–13797.

[46] Sadakane, M.; Dickman, M. H.; Pope, M. T. Controlled assembly of polyoxometalate chains from lacunary building blocks and lanthanide-cation linkers. *Angew. Chem., Int. Ed.* **2000**, *39*, 2914–2916.

[47] Ibrahim, M.; Mbomekallé, I. M.; De Oliveira, P.; Baksi, A.; Carter, A. B.; Peng, Y.; Bergfeldt, T.; Malik, S.; Anson, C. E. Syntheses, crystal structure, electrocatalytic, and magnetic properties of the monolanthanide-containing germanotungstates $[Ln(H_2O)_nGeW_{11}O_{39}]^{5-}$ (Ln = Dy, Er, n = 4, 3). *ACS Omega* **2019**, *4*, 21873–21882.

[48] Cañón-Mancisidor, W.; Zapata-Lizama, M.; Hermosilla-Ibáñez, P.; Cruz, C.; Venegas-Yazigi, D.; Espallargas, G. M. Hybrid organic-inorganic mononuclear lanthanoid single ion magnets. *Chem. Commun. (Camb.)* **2019**, *55*, 14992–14995.

[49] Jing, J. X.; Shi, N.; Sun, Y. Q.; Li, X. X.; Zheng, S. T. An inorganic-organic hybrid polyoxotungstogermanate based on $[Ln(\alpha-GeW_{11}O_{39})_2]$ dimer and dimethylammonium: Synthesis, crystal structure and photoluminescence property. *J. Mol. Struct.* **2022**, *1250*, 131686.

[50] Mougharbel, A. S.; Bhattacharya, S.; Bassil, B. S.; Rubab, A.; Van Leusen, J.; Kögerler, P.; Wojciechowski, J.; Kortz, U. Lanthanide-containing 22-tungsto-2-germanates $[Ln(GeW_{11}O_{39})_2]^{13-}$: Synthesis, structure, and magnetic properties. *Inorg. Chem.* **2020**, *59*, 4340–4348.

[51] Wan, R.; Ma, P. T.; Han, M. D.; Zhang, D. D.; Zhang, C.; Niu, J. Y.; Wang, J. P. Discovery and isolation of the trans-isomers of two 1:2-type lanthanide-containing monolacunary Dawson-type tungstophosphates: $[Ln^{III}(\alpha_2-P_2W_{17}O_{61})_2]^{17-}$ (Ln = La, Ce). *Dalton Trans.* **2017**, *46*, 5398–5405.

[52] Tanuhadi, E.; Al-Sayed, E.; Roller, A.; Čipčić-Paljetak, H.; Verbanac, D.; Rompel, A. Synthesis, characterization, and phosphoesterase activity of a series of 4f- and 4d-sandwich-type germanotungstates $[(n-C_4H_9)_4N]_{l/m}H_2[(M(H_2O)_3)(\gamma-GeW_{10}O_{35})_2]$ (M = Ce^{III}, Nd^{III}, Gd^{III}, Er^{III}, l = 7; Zr^{IV}, m = 6). *Inorg. Chem.* **2020**, *59*, 14078–14084.

[53] Wang, W. Y.; Izarova, N. V.; Van Leusen, J.; Kögerler, P. Ce^{III}-functionalized polyoxotungstates: Discrete vs. extended architectures. *Cryst. Growth Des.* **2019**, *19*, 4860–4870.

[54] Liu, L. Z.; Li, F. Y.; Xu, L.; Liu, X. Z.; Gao, G. G. Magnetic relaxation behavior of lanthanide substituted Dawson-type tungstoarsenates. *J. Solid State Chem.* **2010**, *183*, 350–355.

[55] Huo, Y.; Chen, Y. C.; Wu, S. G.; Liu, J. L.; Jia, J. H.; Chen, W. B.; Wang, B. L.; Zhang, Y. Q.; Tong, M. L. Effect of bridging ligands on magnetic behavior in dinuclear dysprosium cores supported by polyoxometalates. *Inorg. Chem.* **2019**, *58*, 1301–1308.

[56] Ibrahim, M.; Baksi, A.; Peng, Y.; Al-Zeidaneen, F. K.; Mbomekalle, I. M.; De Oliveira, P.; Anson, C. E. Synthesis, characterization, electrochemistry, photoluminescence and magnetic properties of a dinuclear erbium(III)-containing monolacunary dawson-type tungstophosphate: $[\{Er(H_2O)(CH_3COO)(P_2W_{17}O_{61})\}_2]^{16-}$. *Molecules* **2020**, *25*, 4229.

[57] Liu, J. C.; Yu, J.; Han, Q.; Wen, Y.; Chen, L. J.; Zhao, J. W. First quadruple-glycine bridging mono-lanthanide-substituted borotungstate hybrids. *Dalton Trans.* **2016**, *45*, 16471–16484.

[58] Ma, P. T.; Hu, F.; Wu, H. C.; Liu, X. P.; Wang, J. P.; Niu, J. Y. Luminescent dimeric polyoxotungstate $[Ho(C_4H_2O_6)(\alpha-PW_{11}O_{39})]_2^{16-}$ with magnetism and reversible photochromism. *J. Lumin.* **2020**, *217*, 116760.

[59] Niu, J. Y.; Wang, K. H.; Chen, H. N.; Zhao, J. W.; Ma, P. T.; Wang, J. P.; Li, M. X.; Bai, Y.; Dang, D. B. Assembly chemistry between lanthanide cations and monovacant keggin polyoxotungstates: Two types of lanthanide substituted phosphotungstates $[\{(\alpha-$

PW$_{11}O_{39}H)Ln(H_2O)_3\}_2]^{6-}$ and $[\{(\alpha-PW_{11}O_{39})Ln(H_2O)(\eta^2,\mu-1,1)-CH_3COO\}_2]^{10-}$. *Cryst. Growth Des.* **2009**, *9*, 4362–4372.

[60] Wang, X. H.; Liu, Y. J.; Jin, M. T.; Wu, Y. X.; Chen, L. J.; Zhao, J. W. Two families of rare-earth-substituted dawson-type monomeric and dimeric phosphotungstates functionalized by carboxylic ligands. *Cryst. Growth Des.* **2017**, *17*, 5295–5308.

[61] Zhang, S. W.; Wang, Y.; Zhao, J. W.; Ma, P. T.; Wang, J. P.; Niu, J. Y. Two types of oxalate-bridging rare-earth-substituted Keggin-type phosphotungstates $\{[(\alpha-PW_{11}O_{39})RE(H_2O)]_2(C_2O_4)\}^{10-}$ and $\{(\alpha-x-PW_{10}O_{38})RE_2(C_2O_4)(H_2O)_2\}^{3-}$. *Dalton Trans.* **2012**, *41*, 3764–3772.

[62] Knoth, W. H.; Domaille, P. J.; Harlow, R. L. Heteropolyanions of the types $M_3(W_9PO_{34})_2^{12-}$ and $MM'M''(W_9PO_{34})_2^{12-}$: Novel coordination of nitrate and nitrite. *Inorg. Chem.* **1986**, *25*, 1577–1584.

[63] Tomsa, A. R.; Muresan, L.; Koutsodimou, A.; Falaras, P.; Rusu, M. Synthesis and characterisation of two new lanthanide sandwich-type heteropolyoxometalates. *Polyhedron* **2003**, *22*, 2901–2909.

[64] Giansiracusa, M. J.; Vonci, M.; Van Den Heuvel, W.; Gable, R. W.; Moubaraki, B.; Murray, K. S.; Yu, D. H.; Mole, R. A.; Soncini, A.; Boskovic, C. Carbonate-bridged lanthanoid triangles: Single-molecule magnet behavior, inelastic neutron scattering, and *ab initio* studies. *Inorg. Chem.* **2016**, *55*, 5201–5214.

[65] Khoshnavazi, R.; Gholamyan, S. Sandwich-type polyoxoanions based on A-β-GeW$_9O_{34}^{10-}$. Synthesis and characterization of $[(A-\beta-GeW_9O_{34})_2(MOH_2)_3CO_3]^{13-}$ (M = Y^{3+}, Sm^{3+}, and Yb^{3+}) polyoxoanions. *J. Coord. Chem* **2010**, *63*, 3365–3372.

[66] Khoshnavazi, R.; Nicolò, F.; Rudbari, H. A.; Naseri, E.; Aminipour, A. Sandwich-type polyoxometalates of the later lanthanide ions. Syntheses and structures of $[(A-XW_9O_{34})_2(H_2OM)_3CO_3]^{11-}$ (X = P^{5+}, As^{5+}) (M = Tb^{3+}, Dy^{3+}, Er^{3+}). *J. Coord. Chem* **2013**, *66*, 1374–1383.

[67] Khoshnavazi, R.; Sadeghi, R.; Bahrami, L. High stable sandwich-type polyoxometallates based on A-β-SiW$_9O_{34}^{10-}$. Synthesis, chemical properties and characterization of $[(A-\beta-SiW_9O_{34})_2(MOH_2)_3CO_3]^{13-}$ (M = Y^{3+} and Yb^{3+}). *Polyhedron* **2008**, *27*, 1855–1859.

[68] Kong, X. J.; Lin, Z. K.; Zhang, Z. M.; Zhang, T.; Lin, W. B. Hierarchical integration of photosensitizing metal-organic frameworks and nickel-containing polyoxometalates for efficient visible-light-driven hydrogen evolution. *Angew. Chem., Int. Ed.* **2016**, *55*, 6411–6416.

[69] Liu, Y. P.; Zhao, S. F.; Guo, S. X.; Bond, A. M.; Zhang, J.; Zhu, G. B.; Hill, C. L.; Geletii, Y. V. Electrooxidation of ethanol and methanol using the molecular catalyst $[\{Ru_4O_4(OH)_2(H_2O)_4\}(\gamma-SiW_{10}O_{36})_2]^{10-}$. *J. Am. Chem. Soc.* **2016**, *138*, 2617–2628.

[70] Lv, H. J.; Guo, W. W.; Wu, K. F.; Chen, Z. Y.; Bacsa, J.; Musaev, D. G.; Geletii, Y. V.; Lauinger, S. M.; Lian, T. Q.; Hill, C. L. A noble-metal-free, tetra-nickel polyoxotungstate catalyst for efficient photocatalytic hydrogen evolution. *J. Am. Chem. Soc.* **2014**, *136*, 14015–14018.

[71] Yin, Q. S.; Tan, J. M.; Besson, C.; Geletii, Y. V.; Musaev, D. G.; Kuznetsov, A. E.; Luo, Z.; Hardcastle, K. I.; Hill, C. L. A fast soluble carbon-free molecular water oxidation catalyst based on abundant metals. *Science* **2010**, *328*, 342–346.

[72] Dufaye, M.; Duval, S.; Nursiah, K.; Stoclet, G.; Trivelli, X.; Loiseau, T. Bottom-up synthesis of functionalized $\{Ce_4(SiW_9O_{34})_2^{(L)}_2\}$ polyoxometalates. *CrystEngComm* **2018**, *20*, 7144–7155.

[73] Duval, S.; Béghin, S.; Falaise, C.; Trivelli, X.; Rabu, P.; Loiseau, T. Stabilization of tetravalent 4f (Ce), 5d (Hf), or 5f (Th, U) clusters by the $[\alpha-SiW_9O_{34}]^{10-}$ polyoxometalate. *Inorg. Chem.* **2015**, *54*, 8271–8280.

[74] Cai, Z. W.; Liu, B. X.; Yang, T.; Li, X. X.; Zheng, S. T. Syntheses and structures of the first two tetra-scandium substituted polyoxometalates. *Inorg. Chem. Commun.* **2017**, *80*, 1–5.

[75] Wang, Y.; Sun, X. P.; Li, S. Z.; Ma, P. T.; Wang, J. P.; Niu, J. Y. Synthesis and magnetic properties of tartrate-bridging rare-earth-containing polytungstoarsenate aggregates from an adaptive

precursor [As$_2$W$_{19}$O$_{67}$(H$_2$O)]$^{14-}$. *Dalton Trans.* **2015**, *44*, 733–738.

[76] Suzuki, K.; Tang, F.; Kikukawa, Y.; Yamaguchi, K.; Mizuno, N. Visible-light-induced photoredox catalysis with a tetracerium-containing silicotungstate. *Angew. Chem., Int. Ed.* **2014**, *53*, 5356–5360.

[77] Fang, X. K.; Anderson, T. M.; Benelli, C.; Hill, C. L. Polyoxometalate-supported Y- and Yb^{III}-hydroxo/oxo clusters from carbonate-assisted hydrolysis. *Chem.—Eur. J.* **2005**, *11*, 712–718.

[78] Zhang, Y.; Li, Y. M.; Pang, J. J.; Liu, Y. F.; Li, P.; Chen, L. J.; Zhao, J. W. Two penta-RE^{III} encapsulated tetravacant dawson selenotungstates and nanoscale derivatives and their luminescence properties. *Inorg. Chem.* **2019**, *58*, 7078–7090.

[79] Huo, Y.; Chen, Y. C.; Wu, S. G.; Jia, J. H.; Chen, W. B.; Liu, J. L.; Tong, M. L. pH-controlled assembly of organophosphonate-bridged dysprosium(III) single-molecule magnets based on polyoxometalates. *Inorg. Chem* **2018**, *57*, 6773–6777.

[80] Ma, P. T.; Wan, R.; Wang, Y. Y.; Hu, F.; Zhang, D. D.; Niu, J. Y.; Wang, J. P. Coordination-driven self-assembly of a 2D graphite-like framework constructed from high-nuclear Ce$_{10}$ cluster encapsulated polyoxotungstates. *Inorg. Chem.* **2016**, *55*, 918–924.

[81] Ma, P. T.; Wan, R.; Si, Y. N.; Hu, F.; Wang, Y. Y.; Niu, J. Y.; Wang, J. P. Double-malate bridging tri-lanthanoid cluster encapsulated arsenotungstates: Syntheses, structures, luminescence and magnetic properties. *Dalton Trans.* **2015**, *44*, 11514–11523.

[82] Hao, Y.; Zhong, L.; Li, H. H.; Zheng, S. T. Two lanthanide-substituted polyoxometalates featuring novel crescent-shaped Ln$_5$ clusters: Structures, ion conductivities, and magnetic properties. *Cryst. Growth Des.* **2019**, *19*, 1329–1335.

[83] Huo, Y.; Chen, Y. C.; Liu, J. L.; Jia, J. H.; Chen, W. B.; Wu, S. G.; Tong, M. L. A wheel-shaped Dy(III) single-molecule magnet supported by polyoxotungstates. *Dalton Trans.* **2017**, *46*, 16796–16801.

[84] Dufaye, M.; Duval, S.; Stoclet, G.; Loiseau, T. Influence of pH on Ce^{IV}-[As^{III}W$_9$O$_{33}$]$^{9-}$ association for the formation of hexanuclear cerium(IV) oxo-hydroxo-clusters stabilized by trivacant polyanions. *CrystEngComm* **2020**, *22*, 371–380.

[85] Duval, S.; Roussel, P.; Loiseau, T. Synthesis of a large dodecameric cerium cluster stabilized by the [SiW$_9$O$_{34}$]$^{10-}$ polyoxometalate. *Inorg. Chem. Commun.* **2017**, *83*, 52–54.

[86] Matsunaga, S.; Inoue, Y.; Mihara, K.; Nomiya, K. Synthesis and crystal structure of hexacerium(IV) cluster-containing Keggin polyoxometalate trimer. *Inorg. Chem. Commun.* **2017**, *80*, 61–64.

[87] Huo, Y.; Wan, R.; Ma, P. T.; Liu, J. L.; Chen, Y. C.; Li, D. D.; Niu, J. Y.; Wang, J. P.; Tong, M. L. Organophosphonate-bridged polyoxometalate-based dysprosium (III) single-molecule magnet. *Inorg. Chem.* **2017**, *56*, 12687–12691.

[88] Ma, X. Y.; He, P. P.; Xu, B. J.; Lu, J. K.; Wan, R.; Wu, H. C.; Wang, Y.; Ma, P. T.; Niu, J. Y.; Wang, J. P. Pyrazine dicarboxylate-bridged arsenotungstate: Synthesis, characterization, and catalytic activities in epoxidation of olefins and oxidation of alcohols. *Dalton Trans.* **2019**, *48*, 12956–12963.

[89] Ritchie, C.; Baslon, V.; Moore, E. G.; Reber, C.; Boskovic, C. Sensitization of lanthanoid luminescence by organic and inorganic ligands in lanthanoid-organic-polyoxometalates. *Inorg. Chem.* **2012**, *51*, 1142–1151.

[90] Ritchie, C.; Speldrich, M.; Gable, R. W.; Sorace, L.; Kögerler, P.; Boskovic, C. Utilizing the adaptive polyoxometalate [As$_2$W$_{19}$O$_{67}$(H$_2$O)]$^{14-}$ to support a polynuclear lanthanoid-based single-molecule magnet. *Inorg. Chem.* **2011**, *50*, 7004–7014.

[91] Xiong, J.; Yang, Z. X.; Ma, P. T.; Lin, D. M.; Zheng, Q. J.; Huo, Y. pH-controlled assembly of two polynuclear Dy(III)-containing polytungstoarsenates with magnetic and luminescence properties. *Inorg. Chem* **2021**, *60*, 7519–7526.

[92] Chen, H. H.; Xiao, Z. K.; Yan, B.; Wu, H. C.; Ma, P. T.; Wang, J. P.; Niu, J. Y. H-shaped oxalate-bridging lanthanoid-incorporated

[93] Ma, P. T.; Hu, F.; Huo, Y.; Zhang, D. D.; Zhang, C.; Niu, J. Y.; Wang, J. P. Magnetoluminescent bifunctional dysprosium-based phosphotungstates with synthesis and correlations between structures and properties. *Cryst. Growth Des.* **2017**, *17*, 1947–1956.

[94] Howell, R. C.; Perez, F. G.; Jain, S.; Horrocks, W. D. Jr.; Rheingold, A. L.; Francesconi, L. C. A new type of heteropolyoxometalates formed from lacunary polyoxotungstate ions and europium or yttrium cations. *Angew. Chem., Int. Ed* **2001**, *40*, 4031–4034.

[95] Hussain, F.; Gable, R. W.; Speldrich, M.; Kögerler, P.; Boskovic, C. Polyoxotungstate-encapsulated Gd$_6$ and Yb$_{10}$ complexes. *Chem. Commun. (Camb).* **2009**, 328–330

[96] Li, Z.; Li, X. X.; Yang, T.; Cai, Z. W.; Zheng, S. T. Four-shell polyoxometalates featuring high-nuclearity Ln$_{26}$ clusters: Structural transformations of nanoclusters into frameworks triggered by transition-metal ions. *Angew. Chem., Int. Ed.* **2017**, *56*, 2664–2669.

[97] Liu, J. H.; Zhang, R. T.; Zhang, J.; Zhao, D.; Li, X. X.; Sun, Y. Q.; Zheng, S. T. A series of 3D porous lanthanide-substituted polyoxometalate frameworks based on rare hexadecahedral {Ln$_6$W$_8$O$_{28}$} heterometallic cage-shaped cluster. *Inorg. Chem.* **2019**, *58*, 14734–14740.

[98] Wassermann, K.; Dickman, M. H.; Pope, M. T. Self-assembly of supramolecular polyoxometalates: The compact, water-soluble heteropolytungstate anion [As$^{III}_{12}$Ce$^{III}_{16}$(H$_2$O)$_{36}$W$_{148}$O$_{524}$]$^{76-}$. *Angew. Chem., Int. Ed.* **1997**, *36*, 1445–1448.

[99] Jiang, J.; Liu, L. L.; Liu, G. P.; Wang, D.; Zhang, Y.; Chen, L. J.; Zhao, J. W. Organic-inorganic hybrid cerium-encapsulated selenotungstate including three building blocks and its electrochemical detection of dopamine and paracetamol. *Inorg. Chem.* **2020**, *59*, 15355–15364.

[100] Li, H. L.; Lian, C.; Chen, L. J.; Zhao, J. W.; Yang, G. Y. Two unusual nanosized Nd^{3+}-substituted selenotungstate aggregates simultaneously comprising lacunary Keggin and Dawson polyoxotungstate segments. *Nanoscale* **2020**, *12*, 16091–16101.

[101] Li, H. L.; Liu, Y. J.; Li, Y. M.; Chen, L. J.; Zhao, J. W.; Yang, G. Y. Unprecedented selenium and lanthanide simultaneously bridging selenotungstate aggregates stabilized by four tetra-vacant dawson-like {Se$_2$W$_{14}$} units. *Chem.—Asian J.* **2018**, *13*, 2897–2907.

[102] Liu, J. L.; Wang, D.; Xu, X.; Li, H. L.; Zhao, J. W.; Chen, L. J. Multi-nuclear rare-earth-implanted tartaric acid-functionalized selenotungstates and their fluorescent and magnetic properties. *Inorg. Chem.* **2021**, *60*, 2533–2541.

[103] Liu, L. L.; Jiang, J.; Cui, L. M.; Zhao, J. W.; Cao, X. H.; Chen, L. J. Double trigonal pyramidal {SeO$_3$} groups bridged 2-picolinic acid modified cerium-inlaid polyoxometalate including mixed selenotungstate subunits for electrochemically sensing ochratoxin A. *Inorg. Chem.* **2022**, *61*, 1949–1960.

[104] Liu, Y. J.; Li, H. L.; Lu, C. T.; Gong, P. J.; Ma, X. Y.; Chen, L. J.; Zhao, J. W. Organocounterions-assisted and pH-controlled self-assembly of five nanoscale high-nuclear lanthanide substituted heteropolytungstates. *Cryst. Growth Des.* **2017**, *17*, 3917–3928.

[105] Zhang, Y.; Jiang, J.; Liu, Y. F.; Li, P.; Liu, Y.; Chen, L. J.; Zhao, J. W. Multi-praseodymium-and-tungsten bridging octameric tellurotungstate and its 2D honeycomb composite film for detecting estrogen. *Nanoscale* **2020**, *12*, 10842–10853.

[106] Liu, L. L.; Jiang, J.; Liu, X. Y.; Liu, G. P.; Wang, D.; Chen, L. J.; Zhao, J. W. First series of mixed (P^{III}, Se^{IV})-heteroatomoriented rare-earth-embedded polyoxotungstates containing distinct building blocks. *Inorg. Chem. Front.* **2020**, *7*, 4640–4651.

[107] Han, L. Z.; Jiao, C. Q.; Chen, W. C.; Shao, K. Z.; Jin, L. Y.; Su, Z. M. Assembly of tetra-nuclear Yb^{III}-containing selenotungstate clusters: Synthesis, structures, and magnetic properties. *Dalton Trans.* **2021**, *50*, 11535–11541.

[108] Chen, W. C.; Yan, L. K.; Wu, C. X.; Wang, X. L.; Shao, K. Z.; Su, Z. M.; Wang, E. B. Assembly of keggin-/dawson-type

arsenotungstates. *Dalton Trans.* **2020**, *49*, 15731–15738.

polyoxotungstate clusters with different metal units and SeO$_3^{2-}$ heteroanion templates. *Cryst. Growth Des.* **2014**, *14*, 5099–5110.

[109] Han, Q.; Wen, Y.; Liu, J. C.; Zhang, W.; Chen, L. J.; Zhao, J. W. Rare-earth-incorporated tellurotungstate hybrids functionalized by 2-picolinic acid ligands: Syntheses, structures, and properties. *Inorg. Chem.* **2017**, *56*, 13228–13240.

[110] Li, H. L.; Liu, Y. J.; Zheng, R.; Chen, L. J.; Zhao, J. W.; Yang, G. Y. Trigonal pyramidal {AsO$_2$(OH)} bridging tetranuclear rare-earth encapsulated polyoxotungstate aggregates. *Inorg. Chem.* **2016**, *55*, 3881–3893.

[111] Li, H. L.; Lian, C.; Chen, L. J.; Zhao, J. W.; Yang, G. Y. Two Ce^{3+}-substituted selenotungstates regulated by *N,N*-dimethylethanolamine and dimethylamine hydrochloride. *Inorg. Chem.* **2019**, *58*, 8442–8450.

[112] Li, H. L.; Liu, Y. J.; Liu, J. L.; Chen, L. J.; Zhao, J. W.; Yang, G. Y. Structural transformation from dimerization to tetramerization of serine-decorated rare-earth-incorporated arsenotungstates induced by the usage of rare-earth salts. *Chem.—Eur. J.* **2017**, *23*, 2673–2689.

[113] Li, Y. M.; Li, H. L.; Jiang, J.; Chen, L. J.; Zhao, J. W. Three types of distinguishing L-alanine-decorated and rare-earth-incorporated arsenotungstate hybrids prepared in a facile one-step assembly strategy. *Inorg. Chem.* **2019**, *58*, 3479–3491.

[114] Shang, S. X.; Lin, Z. G.; Yin, A. X.; Yang, S.; Chi, Y. N.; Wang, Y.; Dong, J.; Liu, B.; Zhen, N.; Hill, C. L. et al. Self-assembly of Ln(III)-containing tungstotellurates(VI): Correlation of structure and photoluminescence. *Inorg. Chem.* **2018**, *57*, 8831–8840.

[115] Wang, D.; Li, Y. M.; Zhang, Y.; Xu, X.; Liu, Y.; Chen, L. J.; Zhao, J. W. Construction of Ln^{3+}-substituted arsenotungstates modified by 2,5-thiophenedicarboxylic acid and application in selective fluorescence detection of Ba^{2+} in aqueous solution. *Inorg. Chem.* **2020**, *59*, 6839–6848.

[116] Wang, Y. J.; Wu, S. Y.; Sun, Y. Q.; Li, X. X.; Zheng, S. T. Octahedron-shaped three-shell Ln$_{14}$-substituted polyoxotungstogermanates encapsulating a W$_4$O$_{15}$ cluster: Luminescence and frequency dependent magnetic properties. *Chem. Commun. (Camb.)* **2019**, *55*, 2857–2860.

[117] Zhang, Y.; Wang, D.; Zeng, B. X.; Chen, L. J.; Zhao, J. W.; Yang, G. Y. An unprecedented polyhydroxycarboxylic acid ligand bridged multi-Eu^{III} incorporated tellurotungstate and its luminescence propertie. *Dalton Trans.* **2020**, *49*, 8933–8948.

[118] Du, M. H.; Zheng, X. Y.; Kong, X. J.; Long, L. S.; Zheng, L. S. Synthetic protocol for assembling giant heterometallic hydroxide clusters from building blocks: Rational design and efficient synthesis. *Matter* **2020**, *3*, 1334–1349.

[119] Fang, X. K.; Kögerler, P. A polyoxometalate-based manganese carboxylate cluster. *Chem. Commun. (Camb.)* **2008**, 3396–3398

[120] Fang, X. K.; Kögerler, P. PO$_4^{3-}$-mediated polyoxometalate supercluster assembly. *Angew. Chem., Int. Ed.* **2008**, *47*, 8123–8126.

[121] Chen, W. L.; Li, Y. G.; Wang, Y. H.; Wang, E. B.; Zhang, Z. M. A new polyoxometalate-based 3d-4f heterometallic aggregate: A model for the design and synthesis of new heterometallic clusters. *Dalton Trans.* **2008**, 865–867

[122] Gu, Y. N.; Yu, H.; Lin, L. D.; Wu, Y. L.; Li, Z.; Pan, W. Y.; He, J.; Chen, L.; Li, Q.; Li, X. X. Two rare Cr-Ln (Ln = Dy, Tb) heterometallic cluster substituted polyoxometalates featuring hexameric aggregates: Hydrothermal syntheses, crystal structures and magnetic studies. *New J. Chem.* **2019**, *43*, 3011–3016.

[123] Wang, J.; Zhao, J. W.; Zhao, H. Y.; Yang, B. F.; He, H.; Yang, G. Y. Syntheses, structures and properties of two multi-iron-samarium/multi-iron substituted germanotungstates. *CrystEngComm* **2014**, *16*, 252–259.

[124] Zhang, Z. M.; Li, Y. G.; Yao, S.; Wang, E. B. Hexameric polyoxometalates decorated by six 3d-4f heterometallic clusters. *Dalton Trans.* **2011**, *40*, 6475–6479.

[125] Ibrahim, M.; Krämer, S.; Schork, N.; Guthausen, G. Polyoxometalate-based high-spin cluster systems: A NMR relaxivity study up to 14 GHz/33 T. *Dalton Trans.* **2019**, *48*, 15597–15604.

[126] Ibrahim, M.; Mereacre, V.; Leblanc, N.; Wernsdorfer, W.; Anson, C. E.; Powell, A. K. Self-assembly of a giant tetrahedral 3d-4f single-molecule magnet within a polyoxometalate system. *Angew. Chem., Int. Ed.* **2015**, *54*, 15574–15578.

[127] Ibrahim, M.; Peng, Y.; Moreno-Pineda, E.; Anson, C. E.; Schnack, J.; Powell, A. K. Gd$_3$ triangles in a polyoxometalate matrix: Tuning molecular magnetocaloric effects in {Gd$_{30}$M$_8$} polyoxometalate/cluster hybrids through variation of M^{2+}. *Small Struct.* **2021**, *2*, 2170029.

[128] Reinoso, S.; Galán-Mascarós, J. R.; Lezama, L. New type of heterometallic 3d-4f rhomblike core in weakley-like polyoxometalates. *Inorg. Chem.* **2011**, *50*, 9587–9593.

[129] Nohra, B.; Mialane, P.; Dolbecq, A.; Rivière, E.; Marrot, J.; Sécheresse, F. Heterometallic 3d-4f cubane clusters inserted in polyoxometalate matrices. *Chem. Commun. (Camb.)* **2009**, 2703–2705

[130] Wang, W. D.; Li, X. X.; Fang, W. H.; Yang, G. Y. Hydrothermal synthesis and structural characterization of a new keggin-type tungstogermanate containing heterometallic 3d-4f cubane clusters. *J. Cluster Sci.* **2011**, *22*, 87–95.

[131] Wang, Y. F.; Qin, Z. J.; Tian, Z. F.; Bai, Y.; Li, Y. M.; Zhang, Y. W.; Dang, D. B. A series of germanotungstate-based 3d-4f heterometallic compounds with visible-light induced photocatalytic, electrochemical and magnetic properties. *J. Alloys Compd.* **2019**, *784*, 961–969.

[132] Zhao, J. W.; Shi, D. Y.; Chen, L. J.; Li, Y. Z.; Ma, P. T.; Wang, J. P.; Niu, J. Y. Novel polyoxometalate hybrids consisting of copper-lanthanide heterometallic/lanthanide germanotungstate fragments. *Dalton Trans.* **2012**, *41*, 10740–10751.

[133] Cai, J.; Zheng, X. Y.; Xie, J.; Yan, Z. H.; Kong, X. J.; Ren, Y. P.; Long, L. S.; Zheng, L. S. Anion-dependent assembly of heterometallic 3d-4f clusters based on a lacunary polyoxometalate. *Inorg. Chem.* **2017**, *56*, 8439–8445.

[134] Li, S. R.; Wang, H. Y.; Su, H. F.; Chen, H. J.; Du, M. H.; Long, L. S.; Kong, X. J.; Zheng, L. S. A giant 3d-4f polyoxometalate super-tetrahedron with high proton conductivity. *Small Methods* **2021**, *5*, 2000777.

[135] Wu, S. Y.; Wang, Y. J.; Jing, J. X.; Li, X. X.; Sun, Y. Q.; Zheng, S. T. Two organic-inorganic hybrid polyoxotungstogermanates containing organic ligand chelated Fe-Dy heterometallic clusters and frequency dependent magnetic properties. *Inorg. Chem. Front.* **2020**, *7*, 498–504.

[136] Chen, Y.; Guo, Z. W.; Li, X. X.; Zheng, S. T.; Yang, G. Y. Multicomponent cooperative assembly of nanoscale boron-rich polyoxotungstates with 22 and 30 boron atoms. *CCS Chem.* **2022**, *4*, 1305–1314.

[137] Chen, C. H.; Chen, Y.; Yao, R. Q.; Li, Y. X.; Zhang, C. X. Artificial Mn$_4$Ca clusters with exchangeable solvent molecules mimicking the oxygen-evolving center in photosynthesis. *Angew. Chem., Int. Ed.* **2019**, *58*, 3939–3942.

[138] Chen, Y. Z.; Liu, Z. J.; Zhang, Z. M.; Zhou, H. Y.; Zheng, X. T.; Wang, E. B. Systematic assembly of {LnMn$^{III}_4$} appended cubanes with inorganic polyoxometalate ligands and their electrocatalytic property. *Inorg. Chem. Commun.* **2014**, *46*, 155–158.

[139] Yao, R. Q.; Li, Y. X.; Chen, Y.; Xu, B. R.; Chen, C. H.; Zhang, C. X. Rare-earth elements can structurally and energetically replace the calcium in a synthetic Mn$_4$CaO$_4$-cluster mimicking the oxygen-evolving center in photosynthesis. *J. Am. Chem. Soc.* **2021**, *143*, 17360–17365.

[140] Chen, L. J.; Zhang, F.; Ma, X.; Luo, J.; Zhao, J. W. Two types of novel tetra-iron substituted sandwich-type arsenotungastates with supporting lanthanide pendants. *Dalton Trans.* **2015**, *44*,

12598–12612.

[141] Das, V.; Khan, I.; Hussain, F.; Sadakane, M.; Tsunoji, N.; Ichihashi, K.; Kato, C.; Inoue, K.; Nishihara, S. Single-molecule magnetic, catalytic and photoluminescence properties of heterometallic 3d-4f [Ln{PZn₂W₁₀O₃₈(H₂O)₂}₂]¹¹⁻ tungstophosphate nanoclusters. *Eur. J. Inorg. Chem.* **2021**, *2021*, 3819–3831.

[142] Jiang, J.; Chen, Y. H.; Liu, L. L.; Chen, L. J.; Zhao, J. W. 2-Picolinate-decorated iron-lanthanide heterometallic germano-tungstates including an S-shaped [Ge₂W₂₀O₇₂]¹⁶⁻ segment. *Inorg. Chem.* **2019**, *58*, 15853–15863.

[143] Li, S. R.; Weng, Z. Z.; Jiang, L. P.; Wei, R. J.; Su, H. F.; Long, L. S.; Zheng, L. S.; Kong, X. J. A series of heterometallic 3d-4f polyoxometalates as single-molecule magnets. *Chin. Chem. Lett.* **2023**, *34*, 107251–107254.

[144] Minato, T.; Salley, D.; Mizuno, N.; Yamaguchi, K.; Cronin, L.; Suzuki, K. Robotic stepwise synthesis of hetero-multinuclear metal oxo clusters as single-molecule magnets. *J. Am. Chem. Soc.* **2021**, *143*, 12809–12816.

[145] Sato, R.; Suzuki, K.; Minato, T.; Yamaguchi, K.; Mizuno, N. Sequential synthesis of 3d-3d′-4f heterometallic heptanuclear clusters in between lacunary polyoxometalates. *Inorg. Chem.* **2016**, *55*, 2023–2029.

[146] Zhu, S. L.; Xu, X.; Ou, S.; Zhao, M.; He, W. L.; Wu, C. D. Assembly of a metalloporphyrin-polyoxometalate hybrid material for highly efficient activation of molecular oxygen. *Inorg. Chem.* **2016**, *55*, 7295–7300.

[147] Zhao, J. W.; Cao, J.; Li, Y. Z.; Zhang, J.; Chen, L. J. First tungstoantimonate-based transition-metal-lanthanide heterometallic hybrids functionalized by amino acid ligands. *Cryst. Growth Des.* **2014**, *14*, 6217–6229.

[148] Cai, J.; Ye, R.; Liu, X. H.; Guo, L. L.; Qiao, X. R. Ionic strength effect on regulating the synthetic assembly of polyoxometalate clusters with slow magnetic relaxation behavior. *Dalton Trans.* **2020**, *49*, 16954–16961.

[149] Das, V.; Khan, I.; Hussain, F.; Sadakane, M.; Hageo, K.; Ichihashi, K.; Inoue, K.; Nishihara, S. A self-assembled heterometallic {Co₇-Ho₁} nanocluster: 3d-4f trimeric keggin-type silicotungstate [HoCo₇Si₃W₂₉O₁₀₈(OH)₅(H₂O)₄]¹⁸⁻ and its catalytic and magnetic applications. *Eur. J. Inorg. Chem.* **2019**, *2019*, 430–436.

[150] Tanuhadi, E.; Al-Sayed, E.; Novitchi, G.; Roller, A.; Giester, G.; Rompel, A. Cation-directed synthetic strategy using 4f tungstoantimonates as nonlacunary precursors for the generation of 3d-4f clusters. *Inorg. Chem.* **2020**, *59*, 8461–8467.

[151] Gu, Y. N.; Chen, Y.; Wu, Y. L.; Zheng, S. T.; Li, X. X. A series of banana-shaped 3d-4f heterometallic cluster substituted polyoxometalates: Syntheses, crystal structures, and magnetic properties. *Inorg. Chem.* **2018**, *57*, 2472–2479.

[152] Han, Q.; Li, Z.; Liang, X. M.; Ding, Y.; Zheng, S. T. Synthesis of a 6-nm-long transition-metal-rare-earth-containing polyoxometalate. *Inorg. Chem.* **2019**, *58*, 12534–12537.

[153] Yao, M. Y.; Liu, Y. F.; Li, X. X.; Yang, G. P.; Zheng, S. T. The largest Se-4f cluster incorporated polyoxometalate with high Lewis acid-base catalytic activity. *Chem. Commun. (Camb.)* **2022**, *58*, 5737–5740.

[154] Xiao, H. P.; Zhang, R. T.; Li, Z.; Xie, Y. F.; Wang, M.; Ye, Y. D.; Sun, C.; Sun, Y. Q.; Li, X. X.; Zheng, S. T. Organoamine-directed assembly of 5p-4f heterometallic cluster substituted polyoxometalates: Luminescence and proton conduction properties. *Inorg. Chem.* **2021**, *60*, 13718–13726.

[155] Xu, X.; Chen, Y. H.; Zhang, Y.; Liu, Y. F.; Chen, L. J.; Zhao, J. W. Rare-earth and antimony-oxo clusters simultaneously connecting antimonotungstates comprising divacant and tetravacant keggin fragments. *Inorg. Chem.* **2019**, *58*, 11636–11648.

[156] Li, H. L.; Xu, X.; Tang, Z. G.; Zhao, J. W.; Chen, L. J.; Yang, G. Y. Three lanthanide-functionalized antimonotungstate clusters with a {Sb₄O₄Ln₃(H₂O)₈} core: Syntheses, structures, and properties. *Inorg. Chem.* **2021**, *60*, 18065–18074.

[157] Xiao, H. P.; Hao, Y. S.; Li, X. X.; Xu, P.; Huang, M. D.; Zheng, S. T. A water-soluble antimony-rich polyoxometalate with broad-spectrum antitumor activities. *Angew. Chem., Int. Ed.* **2022**, *61*, e202210019.

[158] Xu, X.; Liu, X. Y.; Wang, D.; Liu, X. J.; Chen, L. J.; Zhao, J. W. {HPO₃} and {WO₄} simultaneously induce the assembly of tri-Ln(III)-incorporated antimonotungstates and their photoluminescence behaviors. *Inorg. Chem* **2021**, *60*, 1037–1044.

[159] Xu, X.; Meng, R. R.; Lu, C. T.; Mei, L.; Chen, L. J.; Zhao, J. W. Acetate-decorated tri-Ln(III)-containing antimonotungstates with a tetrahedral {WO₄} group as a structure-directing template and their luminescence properties. *Inorg. Chem.* **2020**, *59*, 3954–3963.

[160] Shao, D.; Wang, X. Y. Development of single-molecule magnets. *Chin. J. Chem.* **2020**, *38*, 1005–1018.

[161] Cardona-Serra, S.; Clemente-Juan, J. M.; Coronado, E.; Gaita-Ariño, A.; Camón, A.; Evangelisti, M.; Luis, F.; Martínez-Pérez, M. J.; Sesé, J. Lanthanoid single-ion magnets based on polyoxometalates with a 5-fold symmetry: The series [LnP₅W₃₀O₁₁₀]¹²⁻ (Ln³⁺ = Tb, Dy, Ho, Er, Tm, and Yb). *J. Am. Chem. Soc.* **2012**, *134*, 14982–14990.

[162] Liu, J. L.; Chen, Y. C.; Tong, M. L. Symmetry strategies for high performance lanthanide-based single-molecule magnets. *Chem. Soc. Rev.* **2018**, *47*, 2431–2453.

[163] AlDamen, M. A.; Clemente-Juan, J. M.; Coronado, E.; Martí-Gastaldo, C.; Gaita-Ariño, A. Mononuclear lanthanide single-molecule magnets based on polyoxometalates. *J. Am. Chem. Soc.* **2008**, *130*, 8874–8875.

[164] Osamu, N.; Teruo, K.; Isao, O.; Yoshizo, M. High-conductivity solid proton conductors: Dodecamolybdophosphoric acid and dodecatungstophosphoric acid crystals. *Chem. Lett.* **1979**, *8*, 17–18.

[165] Liu, J. C.; Han, Q.; Chen, L. J.; Zhao, J. W.; Streb, C.; Song, Y. F. Aggregation of giant cerium-bismuth tungstate clusters into a 3D porous framework with high proton conductivity. *Angew. Chem., Int. Ed.* **2018**, *57*, 8416–8420.

Shu-Rong Li is currently a Ph.D. candidate in the College of Chemistry and Chemical Engineering at Xiamen University. She received her bachelor's degree from School of Chemistry and Material Science of Shanxi Normal University in 2016 and received her master's degree from the College of Chemistry and Chemical Engineering of Xiamen University in 2019. Her research is mainly focused on the synthesis, assembly and properties of polyoxometalates-based lanthanide-oxo clusters.

Wei-Dong Liu is currently a Ph.D. candidate in the College of Chemistry and Chemical Engineering at Xiamen University. He received his bachelor's degree from the School of Chemistry and Chemical Engineering of Henan Normal University in 2020. His research activities have involved the synthesis, structures and properties of lanthanide-titanium-oxo clusters.

La-Sheng Long received his B.S. and M.S. in Chemistry from Anhui Normal University in 1986 and Lanzhou University in 1989, respectively, and his Ph.D. from Zhongshan University in 1999. He is now a professor at Xiamen University. His current research is focused on the synthetic and materials chemistry of cluster compounds containing lanthanide and/or transition metal elements.

Xiang-Jian Kong received his B.S. in Chemistry from Liaocheng University and his Ph.D. from Xiamen University in 2009. He is now a professor at Xiamen University. His research is focused on lanthanide-containing clusters.

Lan-Sun Zheng received his B.S. in chemistry from Xiamen University in China and his Ph.D. from Rice University in 1986 with Professor Richard E. Smalley. He is a professor at Xiamen University.